



Discriminating isotrigrion textures

T. Maddess^{a,*}, Y. Nagai^b

^a Centre for Visual Sciences, Research School of Biological Sciences, Australian National University, Canberra ACT 0200, Australia

^b Center for Information Science, Kokushikan University, Tokyo, Japan

Received 30 November 2000; received in revised form 24 April 2001

Abstract

Higher order spatial correlations can capture edge and object relationships. Isotrigrion textures are useful for studying our sensitivity to these correlations. We determined human discrimination performance for 18 isotrigrion texture types and compared it with outputs from statistical discriminant models. Some of the models employed versions of the Allan Variance in receptive field outputs. Physiologically plausible mechanisms for such calculations are presented. Two discriminant models emulated human performance well, one based upon a global variance measure, and the other based upon a localised variance with an orientation bias. The 18 texture types were also shown to contain characteristic mini-textures. © 2001 Elsevier Science Ltd. All rights reserved.

Keywords: Texture; Isotrigrion; Isodipole; Allan variance

1. Introduction

Beck, Sutter, and Ivry, (1987) showed that a trade-off between texture element size and contrast that affects texture segregation (Beck, 1983) could be explained by spatial summation within oriented narrow-band spatial frequency channels whose output was later full-wave rectified (Sutter, Beck, & Graham, 1989) (by full-wave rectification we mean that the units give similar responses to contrasts that are brighter or darker than average). These so-called 'complex channels', are now well accepted (Landy & Bergen, 1991; Graham, Sutter, Venkatesan, & Humaran, 1992; Graham & Sutter, 1996, 1998, 2000). Experiments on texture defined motion also indicate the presence of a 'texture grabber' based on rectified, oriented spatial filters (Chubb & Sperling 1991), where the extracted textural information may form the input to the same motion detecting mechanism as that for luminance defined motion (Turano & Pantle, 1989; Werkhoven, Sperling, & Chubb, 1993, 1994). Nonlinear mechanisms also appear to underlie texture

discrimination on the basis of orientation modulation (Kingdom, Keeble, & Moulden, 1995).

Julesz, Gilbert, Shep, and Frisch (1973) hypothesised that humans could not discriminate briefly presented textures whose second order correlation functions were the same, so called *isodipole* textures (for summary see Julesz, 1980). While Julesz and colleagues used slightly different statistics to the standard autocorrelation function the two statistics are the same providing the compared textures have the same mean luminance (Klein & Tyler, 1986). Discriminable isodipole patterns were soon found (Caelli & Julesz, 1978; Caelli, Julesz, & Gilbert, 1978; Caelli & Julesz, 1979). Finally, a class of patterns were found which, although easily discriminable, had group averaged third order correlation functions that are the same (Julesz, Gilbert, & Victor, 1978), i.e. correlation functions based on triplets of image points. Such collections of *isotrigrion* textures by definition also have, on average, the same means and second order correlations, that is, they are also isodipole (Gilbert, 1980), and several such textures have now been investigated (Gilbert, 1980; Victor & Conte, 1991). While the third order correlation function of any monochromatic image uniquely determines that image (Yellott, 1993) ensemble averages of groups of isotrigrion textures have third order correlation functions that are also

* Corresponding author. Tel.: + 61-2-6249-4099; fax: + 61-2-6249-3808.

E-mail address: ted.maddess@anu.edu.au (T. Maddess).

indiscriminable from that of binary noise (Victor, 1994). Hence, the average third order correlation functions of collections of isotrigran textures cannot, on average, be used to discriminate other collections of differing types of isotrigran textures. It is worth noting that ensembles of several textures need to be averaged to achieve good isotrigranity (Gagalowicz, 1981). We have therefore used large collections of textures here so that what discriminates them on average cannot be their third or lower order statistics.

Purpura, Victor, and Katz (1994) noted that while two-point correlations inform the visual system about the (phase independent) spatial frequency content of images, encoding features such as contours requires mechanisms sensitive to correlations involving three or more points. VEP studies with isotrigran stimuli have shown that the visual cortex does utilise higher order correlations (Victor, 1985; Victor & Zemon, 1985; Victor & Conte, 1989, 1991). Seventy percent of single units in macaque V1 have been shown to encode such high order statistical information, and this ability is not dependent on cortical layer (Purpura et al.). PET (Beason-Held et al., 1998b) and fMRI (Beason-Held et al., 1998a; Beason-Held et al., 2000) studies have revealed brain regions specialising in discriminating random from isotrigran patterns.

The isotrigran textures used to date each have two related forms, the so-called Even and Odd variants. The studies mentioned above have used one isotrigran texture class, the Even and Odd patterns generated by the 2×2 Box glider (Fig. 1, column 1) and some variants. One study (Victor & Conte, 1991) has examined discrimination of Random binary textures from modified versions of the nine Even textures used here. Given the interesting possibilities for using isotrigran textures in studying vision we sought to quantify discrimination between 27 combinations of Even vs.

Random, Odd vs. Random, and Even vs. Odd textures. These discriminations were quantified for four octaves of texture sizes. We also examined the effect of texture contrast and scale, random number seed, and examined long-term learning effects. Since we were studying discrimination we also sought to compare human performance with that produced by formal statistical discriminant models that shared some features of common texture segregation mechanisms.

Since a quantity known as the Allan Variance has computational similarity to physiological mechanisms for calculating even order nonlinear interactions we explored the use of four versions of Allan Variance as inputs to the discriminant models. These variance measures were based on outputs of localised receptive field models. Linear and quadratic discriminant models were considered. Since the variance models supplied second order statistical information the resultant linear and quadratic discriminant models were formally comparing second and fourth order spatial correlations. This provides a test of the idea that neural responses containing these higher order correlations, often modelled as being produced by a cascade of two levels of nonlinear interactions across space, are required for discrimination of textures having similar lower order statistics (Malik & Perona, 1990; Victor & Conte, 1991; see also R ath & Morfill, 1997).

We also examined the local properties of the textures by characterising the number of types of small 3×3 and 4×4 pixel sub-domains of the textures, which we refer to as mini-textures. We related the characteristic number and form of mini-textures found within each class of the 19 texture types (nine Even, nine Odd and Random) we investigated.

A common method in texture discrimination studies is to embed small samples of one texture within a large background and to examine the degree to which

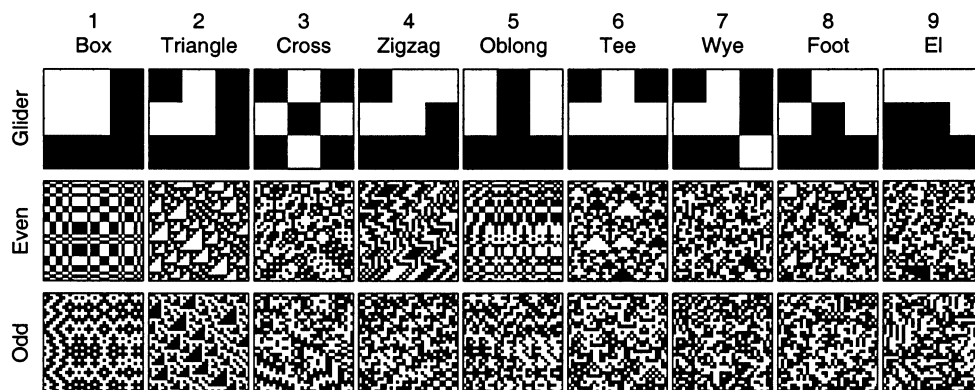


Fig. 1. Examples of the texture types used. The 18 texture types illustrated in the bottom two rows were produced using a recursion rule (Section 2). At the top of each column is a representation of the *glider* used to produce the Even and Odd textures below it. The white block pixels represent the active pixels of the glider (Section 2). Even and Odd textures (rows 2 and 3) being produced by two variants of the recursion rule operated on each glider type. The names of the gliders, and so their related texture types, are shown above along with a numerical reference {1–9} used in placed of the glider names in figures that follow.

the small sample is seen (Julesz, 1981). A problem with this approach is that it can be confounded by (possibly) higher-level mechanisms leading to discrimination asymmetries (Gurnsey & Browse, 1987, 1989; Rubenstein & Sagi, 1990) related to those seen in visual search (Treisman & Gormican, 1988). Finally, the small embedded pattern approach was impractical as we were specifically investigating the effect of texture sample size and its possible interaction with mini-texture content. Therefore, we have taken an experimental approach closer to that of Victor and Conte (1991), the only other study of a substantial subset of the patterns investigated here. Aside from providing easy comparison with related work another motivation for this approach was to try to examine the low-level constraints upon discrimination. This was attempted by providing many trials of a two alternative forced choice method (with feed back) where the presentation time is short enough to permit only a single fixation and target position is fixed. As shown by Geisler and Chou (1995) this methodology reduces, memory load, learning (following much practice with feedback) and attentional effects, allowing better access to low-level constraints. Thus, the present study provides the basis for future studies in which the ability of our data to predict embedded texture discrimination and or visual search could be contemplated.

2. Methods

2.1. Stimuli

Achromatic (colour temperature 6500 K) texture patterns were displayed at mean luminance of 45 cpd m^{-2} on a Barco CCID 7551 monitor at a pixel resolution of 512×420 square pixels, and a refresh rate of 101 Hz. The ambient illumination was that provided by the monitor in an otherwise darkened room. Monitor linearity was confirmed by nonlinear systems identification methods (Maddess, James, Goldberg, Wine, & Dobinson, 2000). Subjects viewed the patterns binocularly from a distance of 60 cm with the aid of a chin rest.

The texture patterns used here include random binary textures and the nine classes described by Victor and Conte (1991). For the *random* patterns the probability of a given check being dark or bright was 0.5. The non-random textures were created by a recursion process (Victor & Conte, 1991). To begin the process a matrix is set randomly dark (-1) or bright (1) with probability 0.5. Then checks are then recoloured by a recursion rule operating *via* a moving 3×3 pixel domain. The recursion rule only operates on a subset of the 9 pixels, the shape of these active pixels being

referred to as a *glider*. Nine different gliders define the nine textural types used here (Fig. 1). Each glider can generate two related types of texture known as the *Even* and *Odd* versions. For example, to produce Even textures from 4 pixel gliders the 4th pixel is set equal to the product of the other three, and thus the subsequent product with the 4th pixel is always 1. Odd textures are created by inverting the sign of the product of the first three glider elements, and setting the 4th pixel equal to that, so that the product of the 4 glider pixels is -1 . In either case the product of the first 3 pixels determines the value of the fourth. The statistics of the generated pattern does not depend on the initial pixel values or in which direction the recursion is operated (Gilbert, 1980). With the exception of the Triangle texture, ensemble averages of all these texture types have the same third order correlation functions as that for binary noise patterns, and are thus said to be isotrigrion textures (Victor, 1994). By definition this means the patterns also have equal ensemble-averaged second order correlation functions and are thus isodipole textures. Blurring of the patterns can foil their isotrigrion property but does not affect their isodipole property since blurring will have the same affect on the 2-D power spectra, which are the Fourier transforms of the 2-D correlation functions (Victor, 1994). The Triangle textures are only isodipole even without blurring and so they provide an interesting contrast.

Four sizes of textures were employed: 4×4 , 8×8 , 16×16 and 32×32 pixels. Typically the pixel blocks were $58'$ square measured at the CRT centre. Some trials employing textures made with four times smaller blocks ($14.5'$ square) were also conducted. The large block pixels used here minimised the possible effects of blurring. All textures were presented at the CRT centre, the remaining $32 \times 24^\circ$ ($h \times v$) face of the CRT was a blank field at the mean luminance. Within each presentation the contrast of the gratings was increased from 0 to the test contrast and then back down to 0. To minimise the effect of onset and offset transients the leading and trailing five frames of each presentation followed a Blackman function (Blackman & Tukey, 1959): $\text{Blackman}(t) = 0.42 - 0.5 \times \cos(2\pi(t - t_0)/\tau) + 0.08 \times \cos(4\pi(t - t_0)/\tau)$ (Fig. 2). The stimulus was thus on at full contrast for 204 ms and the total stimulus duration was 297 ms (Fig. 2). The quarter-second presentations and windowing insured patterns were seen for a single fixation and where designed to prevent nonlinear spatial distortions of the patterns that has been observed for shorter presentation times (Maddess & Kulikowski, 1999). In most experiments textures were presented at contrast 1 but in some trials contrasts of 0.1 or 0.2 were used.

For a particular block of trials subjects were shown

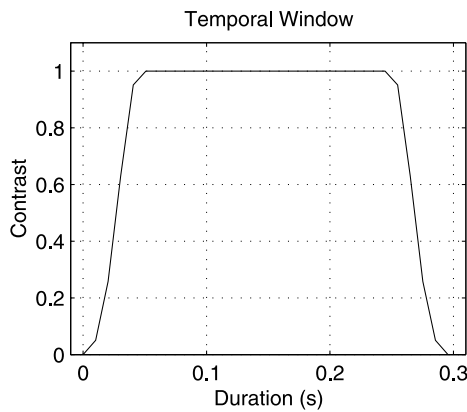


Fig. 2. The temporal function governing the contrast of the textures during each presentation. The sigmoidal onset and offset are determined by a Blackman function (Section 2) and were introduced to reduce nonlinearities associated with abrupt changes in contrast.

either Even or Random textures, Odd or Random textures, or Even or Odd textures, where the non-random textures were drawn using one of the nine gliders and the appropriate Odd or Even rule. These three types of discriminations are henceforth referred to as ER, OR and EO discriminations. Before each block of trials subjects were given printed black and white examples of the textures having 64×64 pixels (15×15 cm) to inspect for up to 3 min (typically < 1 min). Within a given block of trials 12 texture samples of different sizes were presented: first at 32×32 pixels, then 12 textures at 16×16 pixels, and so on to a minimum size of 4×4 pixels. It is important to note that the printed textures were only presented before the first set of trials at 32×32 pixels. In fact these printed reminders proved relatively useless as the large-scale structure apparent in these patterns is not evident in the smaller samples, and subjects had to rely upon feedback to learn the discriminations. Subjects indicated by a mouse button-press whether a given texture was Even or Random, Odd or Random, or Even or Odd, depending on the type of trial being conducted. Incorrect choices were indicated by a tone. Blocks of trials for each glider texture class were completed in the order ER, OR, EO. Blocks of trials for the textures generated by the nine different gliders were completed at random providing 27 ($\times 12$) discriminations each for up to four texture sizes. Two subjects (TM, YN) completed five repeats of the entire process, partly to study long term learning, and partly to test a few subjects with textures generated from several different random number seeds.

2.2. Statistics

We employed both linear and quadratic discriminant analyses (Johnson & Wichern, 1992) to attempt

to mimic the human discrimination process within a statistical formalism. In the linear discriminant case the covariances S are assumed to be equal and are pooled, $S_{\text{pooled}} = ((m-1)S_1 + (n-1)S_2)/(m+n-2)$ to obtain a better estimate. If we have two multivariate normal populations π_1 and π_2 the condition for assigning an observation x_0 to π_1 , for the case of equal prior odds of encountering π_1 or π_2 and equal costs for mis-classification as π_1 or π_2 , is:

$$(\mathbf{u}_1 - \mathbf{u}_2)' S^{-1} x_0 + \frac{1}{2} \mathbf{u}_2' S^{-1} \mathbf{u}_2 - \frac{1}{2} \mathbf{u}_1' S^{-1} \mathbf{u}_1 > 0, \quad (1)$$

Where the \mathbf{u}_n are the means for π_1 and π_2 , S is the pooled covariance, and x_0 is a sample (vector) to be classified as either being from π_1 and π_2 . This condition can be written in the form,

$$\mathbf{b}x_0 + c > 0, \quad (2)$$

where c is a scalar, and \mathbf{b} is a row vector of coefficients. This is sometimes referred to as Fischer's *linear* discriminant or classification rule.

If the covariance matrices are not equal, i.e. $S_1 \neq S_2$, then the resultant rule is to classify an observation x_0 as being from population Eq. (1) (π_1) if the following quadratic condition holds:

$$x_0' \mathbf{A} x_0 + \mathbf{b}' x_0 + c > 0 \quad (3)$$

where,

$$\mathbf{A} = \frac{1}{2} (S_2^{-1} - S_1^{-1}),$$

$$\mathbf{b} = -\frac{1}{2} (\mathbf{u}_2' S_2^{-1} - \mathbf{u}_1' S_1^{-1}),$$

$$c = \frac{1}{2} (\mathbf{u}_2' S_2^{-1} \mathbf{u}_2 - \mathbf{u}_1' S_1^{-1} \mathbf{u}_1) + \frac{1}{2} \log (\det(S_2)/\det(S_1)).$$

Geometrically, the linear discriminant function defines a decision boundary, or *separatrix*, that is a straight line across the plane in the case of a bivariate observation, and in general is a hyperplane in the multivariate case. The quadratic discriminant rule defines a decision boundary that is a paraboloid in the bivariate case, and is a paraboloidal surface in the general multivariate case (for examples see, Maddess et al., 1999b; Maddess et al., 2000).

2.3. Subjects and general

The authors and three naive subjects were used. All subjects were male and ranged in age between 22 and 49 years and had normal or corrected-to-normal vision. This study was conducted under protocol M881 of the Human Ethics Experimentation Committee of the Australian National University. All calculations were performed using Matlab Release 11 (The Mathworks, Natick, MA), and the random number seeds were set by using the *state* variable of its 'rand' function.

3. Results

3.1. Mini-textures

As a starting point it is reasonable to assume that the visual system may initially perform a local analysis of the textures. This leads to consideration of small two-dimensional domains of the parent textures that we refer to here as mini-textures. For an $N \times M$ pixel binary random mini-texture the possible number of mini-textures is 2^{NM} , hence for a 3×3 domain we obtain $2^9 = 512$, and for 4×4 pixels $2^{16} = 65536$. It can be shown (Appendix A) that for textures like those used here, where the number of active pixels of the glider is less than the total number of pixels in the whole glider domain (3×3 in the present case), that the total number of mini-textures generated by the recursion process will be less than 2^{NM} .

As an empirical check of the idea that the total number of mini-textures will be less than 2^{NM} we took 16 Odd and Even 100 pixel² textures for each of our nine texture/glider types and examined the number and type of unique mini-textures in each (Fig. 2a, b). Each of the 16 examples of the resulting 18 texture types was constructed from a different random

number seed. The $\{-1, 1\}$ textures were converted to $\{0, 1\}$, the columns were concatenated to a single vector, and the resulting binary number was used as an index identifying each unique mini-texture type. The indices were used to create histograms of the number of mini-textures in a given parent texture (Fig. 3c). Notice that for a 3×3 mini-texture there are thus $2^9 = 512$ indices, i.e. one histogram bin for every possible 3×3 mini-texture. The resultant counts were used to form frequency histograms (Fig. 3d) of the number of occurrences of each mini-texture in much larger parent textures. The process was repeated for 4×4 mini-textures. In this case 288 (18 types \times 16 examples) textures were used, each 416 pixel² to insure a sufficient number of each mini-texture was obtained for each of the 65536 possibly valid histogram bins. While the analysis in Appendix A predicts the number of unique mini-textures in each texture type (Tables 1 and A1) it says nothing about the mini-textures that are shared between the various texture types. The above empirical analysis permitted these relationships to be quantified (Table 2, and Fig. 4).

As illustrated by Fig. 3d the histogram of mini-texture frequencies were quite flat but nevertheless showed a structure having mirror symmetry in the

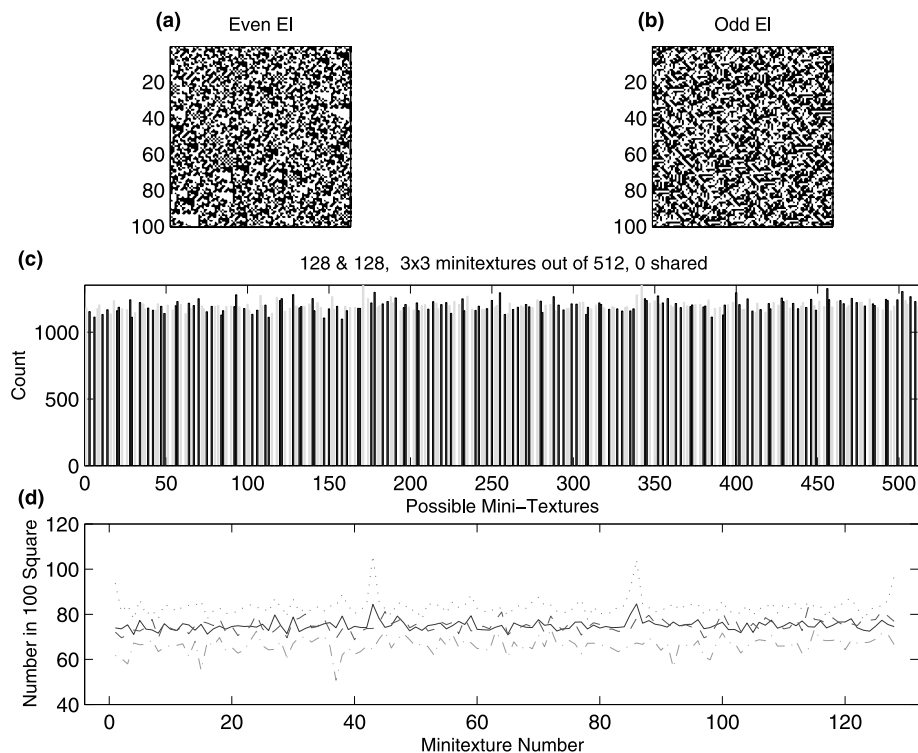


Fig. 3. Illustration of the mini-textures found in Even (a), and Odd (b), EI textures (texture type 9, Fig. 1). The 34848 3×3 pixel mini-textures contained in each of thirty-two 100 pixel² textures generated using 32 different random number seeds were sorted into the 512 possible mini-texture types permitted for 3×3 binary mini-textures. The histogram (c) shows accumulated mini-texture counts for Odd (black bars) and Even (grey bars) versions of EI textures. Each generates 128, mutually exclusive, mini-texture types. (d) The frequency of each mini-texture type per 100 pixel² texture for Even (solid line) and Odd (dashed line) versions. The mean frequency + 1 SD for Even (dotted line), and the mean frequency - 1 SD for Odd (dash dot line) are also shown.

Table 1

The number of mini-textures found for 3×3 and 4×4 pixel domains in each of the nine texture types using the histogram method of Fig. 3

No.	Name	3×3	4×4
1	Box	32	128
2	Triangle	32	128
3	Cross	256	4096
4	Zigzag	128	1024
5	Oblong	128	1024
6	Tee	128	1024
7	Wye	256	4096
8	Foot	128	1024
9	El	128	1024

The number of mini-textures for Odd and Even types of each texture is the same but none of the mini-textures are shared between Odds and Evens (see Table 2c). Data were reproduced for textures generated from 16 different random number seeds and the same mini-textures were observed for each texture type independent of the seeds.

Table 2

The number of *shared* 3×3 mini-textures for the nine texture types

	Box	Tri	Cro	Zig	Obl	Tee	Wye	Foo	El
(a) E^E									
Box	32	4	16	16	32	8	16	16	8
Triangle	4	32	16	8	8	8	16	32	8
Cross	16	16	256	64	64	64	128	64	64
Zigzag	16	8	64	128	32	32	64	32	32
Oblong	32	8	64	32	128	32	64	32	32
Tee	8	8	64	32	32	128	64	32	32
Wye	16	16	128	64	64	64	256	64	64
Foot	16	32	64	32	32	32	64	128	32
El	8	8	64	32	32	32	64	32	128
(b) O^O									
Box	32	0	16	16	0	8	16	0	8
Triangle	0	32	16	8	8	8	16	0	8
Cross	16	16	256	64	64	64	128	64	64
Zigzag	16	8	64	128	32	32	64	32	32
Oblong	0	8	64	32	128	32	64	32	32
Tee	8	8	64	32	32	128	64	32	32
Wye	16	16	128	64	64	64	256	64	64
Foot	0	0	64	32	32	32	64	128	32
El	8	8	64	32	32	32	64	32	128
(c) E^O									
Box	0	4	16	16	0	8	16	16	8
Triangle	0	0	16	8	8	8	16	0	8
Cross	16	16	0	64	64	64	128	64	64
Zigzag	16	8	64	0	32	32	64	32	32
Oblong	32	8	64	32	0	32	64	32	32
Tee	8	8	64	32	32	0	64	32	32
Wye	16	16	128	64	64	64	0	64	64
Foot	0	32	64	32	32	32	64	0	32
El	8	8	64	32	32	32	64	32	0

The column labels are the first three letters of the glider names from Table 1. (a) Number of shared 3×3 textures between Even textures. The diagonal (bold) is the same as column 3 of Table 1. (b) Shared mini-textures between Odd textures. (c) Shared mini-textures between Even and Odd. Notice that the diagonal is all zeros (for an example see Fig. 4).

frequencies of appearance of particular textures. The same symmetry was present in the variance of the frequencies of appearance of particular mini-textures. Frequency histograms for both 3×3 and 4×4 mini-textures from all 18 texture types exhibited this mirrored property although the mirrored patterns differed for different textures. As shown in Table 3 the frequency of mini-textures was similar for Even and Odd texture pairs, but the variance in the frequencies was the same or larger for Even mini-textures. So, for example, for the 3×3 mini-textures taken from 100 pixel² Even Zigzag textures each possible mini-texture occurs 75.0 ± 27.2 SD times, and 75.0 ± 18.0 SD times for Odd Zigzag patterns.

Notice that all the textures should in principle be perfectly discriminable from random textures given that the *alphabet* of 3×3 mini-textures defining any of the 18 texture types used here will never have

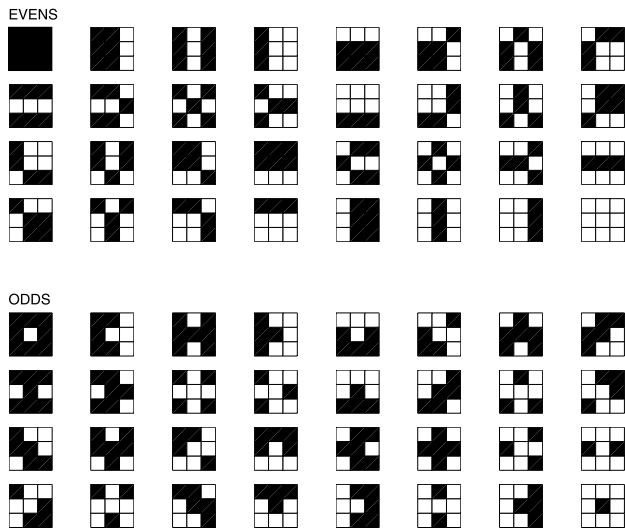


Fig. 4. The 32 mini-textures found in Even (upper four rows) and Odd textures (lower four rows) produced with the Box glider. Notice that each Even mini-texture has a corresponding Odd mini-texture that differs by 1 pixel.

have 512 possible states, R , and the deterministic textures (see Appendix A for definition) we have used are constrained to a lesser number of mini-textures, N (Appendix A, Table 1), then a simple idea would be that discrimination, D , might be $D = 1 - (R - N)/R$. D is plotted as a solid line in Fig. 8b. While D has some features of the psychometric function there is no a priori reason to assume that the frequency of 3×3 mini-textures is especially relevant to discrimination of 4×4 textures.

Since the authors completed five repeats of the all discriminations over the space of several months it is reasonable to look for learning effects. Linear regression across repeats on data for each texture and size showed significant learning in some cases. Fig. 9 sum-

marises the regression data where the 30 data sets per subject (two authors, five repeats, ER, OR, EO) have more than half the *letters* (mini-textures) found in random binary textures. In practice human performance is less than perfect (see below). A possible source of poor performance is spatial summation by receptive fields. A trivial example would be a hypothetical receptive field that summed all the pixels within a 3×3 domain with equal weights, clearly this would produce the same output for every mini-texture having 1 bright and 8 dark pixels and so on. Thus, summation could greatly reduce the number of observable responses compared to the number of mini-textures, even without consideration of noise. Spatial summation may in effect provide humans with a reduced alphabet of mini-textures with which to discriminate binary textures.

3.2. Psychophysics

Since we were interested in the local properties of the textures under study for each texture type subjects made ER, OR and EO discriminations for three or four texture sizes (Section 2) within each block of trials. In the first block of trials textures that were 32×32 pixels presented, and in subsequent trials texture size was reduced in octave steps to as small as 4×4 pixels. Fig. 5 shows the average outcomes for five subjects. Two different random number seeds were used for these data, two subjects viewed textures produced from one seed and the other three subjects viewed textures from a second seed. Discrimination fell generally below the 75% level when texture size was reduced to 8×8 pixels (Fig. 5f), although textures 1 (Box) and 2 (Triangle) continued at near saturated performance levels. The authors completed five repeats for all textures each viewing textures made using five different random number seeds (Fig. 6). The resulting psychometric functions are very similar across subjects and seeds (Figs. 5 and 6). The authors

Table 3
The mean frequency of occurrence (number/(100 × 100 pixel texture)) of 3×3 mini-textures for Even (column 1) and Odd (column 3) versions of the nine texture types

No.	Name	Mean N Even	SD N Even	Mean N Odd	SD N Odd
1	Box	300.1 ± 22.7	82.9 ± 29.8	300.1 ± 15.3	48.6 ± 8.7
2	Triangle	300.1 ± 2.6	15.8 ± 6.6	300.1 ± 2.9	15.8 ± 5.9
3	Cross	37.5 ± 3.0	11.5 ± 3.2	37.5 ± 2.5	8.9 ± 2.0
4	Zigzag	75.0 ± 6.9	27.2 ± 10.7	75.0 ± 5.4	18.0 ± 7.9
5	Oblong	75.0 ± 8.4	26.0 ± 7.9	75.0 ± 3.7	15.6 ± 3.1
6	Tee	75.0 ± 2.2	8.7 ± 2.5	75.0 ± 2.2	8.2 ± 2.5
7	Wye	37.5 ± 1.9	6.2 ± 1.7	37.5 ± 1.3	6.0 ± 1.2
8	Foot	75.0 ± 3.0	16.3 ± 5.8	75.0 ± 2.7	10.6 ± 1.8
9	El	75.0 ± 2.2	8.4 ± 2.7	75.0 ± 2.8	8.7 ± 2.6

The standard deviation in those quantities are also given (columns 2 and 4). Each value in the table has an associated standard deviation (±SD) since they are each an estimate from 16 repeats for textures generated from initial data sets based on 16 different random number seeds.

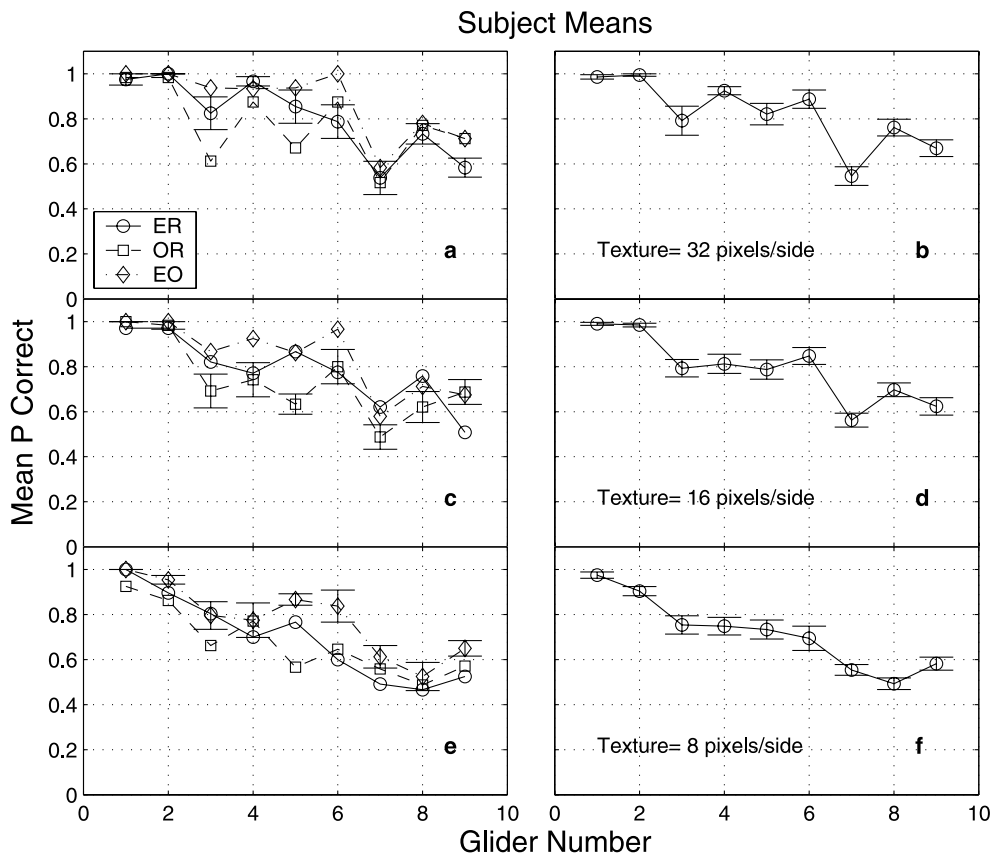


Fig. 5. Average psychometric functions showing the mean probability (P) of correct discriminations from five subjects for ER, OR and EO (a, legend) discriminations (a, c, d) and the averages for three texture sizes types (b, d, f). The top row of panels (a, b) shows data for 32 pixel² textures, the middle (c, d), and bottom rows (e, f) for 16 and 8 pixels², respectively. Texture numbers shown on the abscissa are defined in Fig. 1. Error bars are SE and one set per panel are shown to maximise legibility.

also repeated all the discriminations at two lower contrasts (0.1 and 0.2) and a four times smaller check size. Averages cross both subjects and for different cases are shown in Fig. 7. The averages across discriminations (Figs. 5–7b, d, f) are very similar all having a dips at textures 3 (Cross), 7 (Wye) and 9 (El) (see also Fig. 16).

The authors also completed two repeats of all discriminations (24 repeats per texture and size, for ER, EO, and EO) for 4×4 pixels (Fig. 8). These data were collected in blocks of trials containing the larger texture sizes obtained during the first two repeats of the experiments of Fig. 6. Even for these quite experienced observers performance fell to 65% or lower for all but textures 1 (Box) and 2 (Triangle). A simple model is also shown together with the average discrimination data for the 4×4 pixel case (Fig. 8b). Given that Random binary 3×3 mini-textures can be fitted together. Starred symbols were significant at $P < 0.05$. The significant learning effects were observed for textures 3 (Cross) and 9 (El) at all sizes, and for the larger textures generally. The curves for smaller textures are similar in shape to those for the larger textures suggesting that the lower slopes may contribute to the lack of significance.

3.3. Modelling

Since the task we were examining was the ability of humans to make various textural discriminations we thought it might be useful to explore formal statistical discriminant models as a way of obtaining insights into, or quantifying constraints upon, human performance. We employed Linear Discriminant Analysis (LDA) and Quadratic Discriminant Analysis (QDA) (see Section 2). For two populations, π_1 and π_2 , the object of discriminant analysis is to assign an observation x_0 to one population or the other (Section 2). In our case π_1 and π_2 represent some measures obtained from populations of textural types in an ER, EO or EO comparison. Clearly several measures on each example could be made, for example, some measure for each of the 3×3 mini-textures contained in a 12×12 texture sample. Thus, x_0 is in general a vector $x_0 = \{x_1, x_2, x_3, \dots, x_n\}$. In the case of two-dimensional data, $x_0 = \{x_1, x_2\}$, where the observations and populations span a plane, the object of LDA is to use the covariances and means to define a line or *separatrix*, splitting the plane into two parts where observations will be assigned to either π_1 or π_2 , with the minimum cost (Section 2). For higher

dimensional data the separatrix is a hyperplane. QDA encompasses the case where the population covariances are unequal, $S_1 \neq S_2$, and the separatrix is a paraboloidal surface. As the name suggests QDA expands on LDA by including coefficients estimated for all quadratic interactions between the components of the observations (Eq. (3), Section 2).

A measure that has gained some interest in characterising time series and $1/f^a$ noise is the Allan Variance (Allan, 1966). The Allan Variance has been shown to be equivalent to Wavelet Variance for certain wavelets (Howe & Percival, 1995) where the interest is in examining correlations at different scales. A further possible advantage of Allan Variance over the conventional variance is that it converges to a finite value for most types of noise, whereas the classical variance does not always converge to a finite value. For example, the central-limit theorem does not apply to some chaotic processes (Yamaguchi & Nagai, 1998) and the Allan Variance may be useful in such cases. The conventional Allan Variance is just the half the sum of the squared differences between adjacent points in a one-dimensional series of numbers x_i : $AV = \frac{1}{2} \sum (x_{i+1} - x_i)^2 / N$. The factor of $\frac{1}{2}$ makes the Allan Variance equal to the conventional

variance: $\sum (u - x_i)^2 / N$, (u is the population mean), for Gaussian distributed noise. Note that the AV is composed of the sum of squares of paired linear combinations of inputs of the form $(a - b)^2$. Such combinations represent a neurally plausible means of computing quadratic interactions (Section 4, Fig. 17) between receptive field outputs, that was first proposed for motion detection (Emerson, Bergen, & Adelson, 1992).

In the section on mini-textures above we introduced the idea that the operation of spatial averaging *via* linear receptive field mechanisms would reduce the alphabet of mini-textures available for discrimination of the parent textures. Given that the Allan Variance, or some related measure, might be useful for characterising various types of noise, and given the need to consider receptive field mechanisms, we decided to examine a few variants of the Allan Variance in the receptive field outputs as inputs to our discriminant analyses. To do this we introduced square 'receptive fields', r , of various pixel sizes and spatial weightings. We then performed an operation akin to a convolution: calculating the mean output for the product of the receptive field weights with each pixel of the corresponding sized mini-texture m for positions

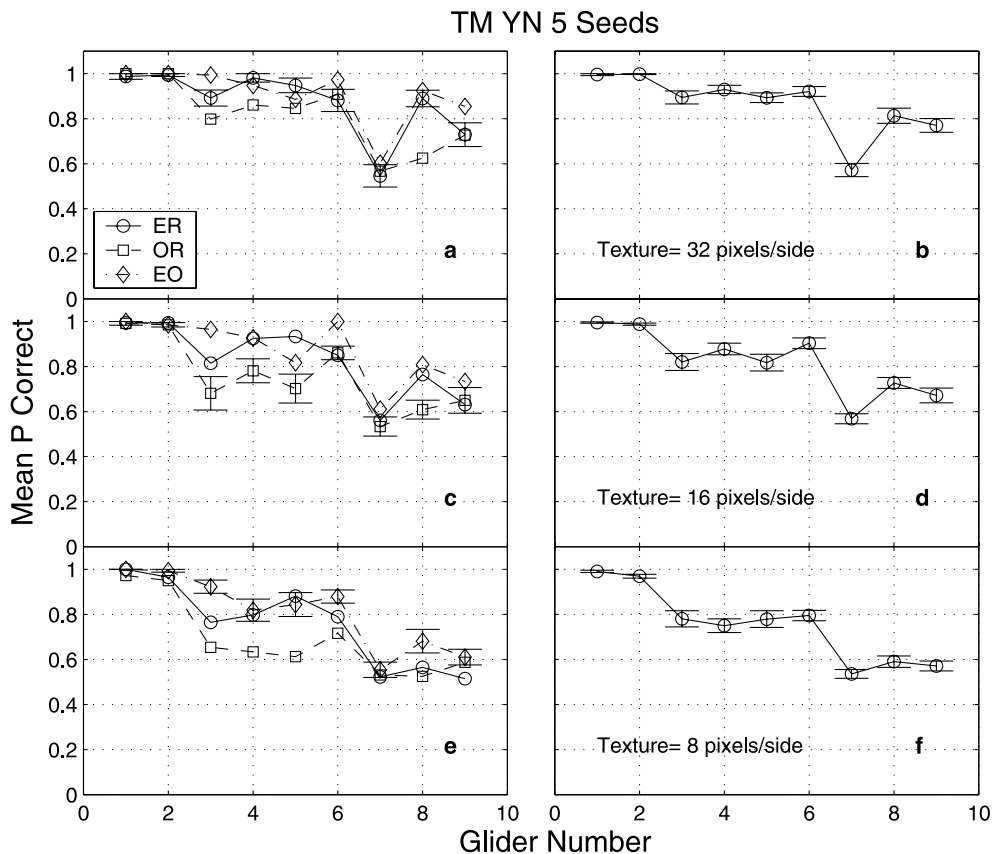


Fig. 6. As for Fig. 5 but the data are averages of from five repeats by each of the authors (10 data sets in all). Different seeds for the random number generator (Section 2) were used for each of the five tested sets of textures. Conventions as in Fig. 5.

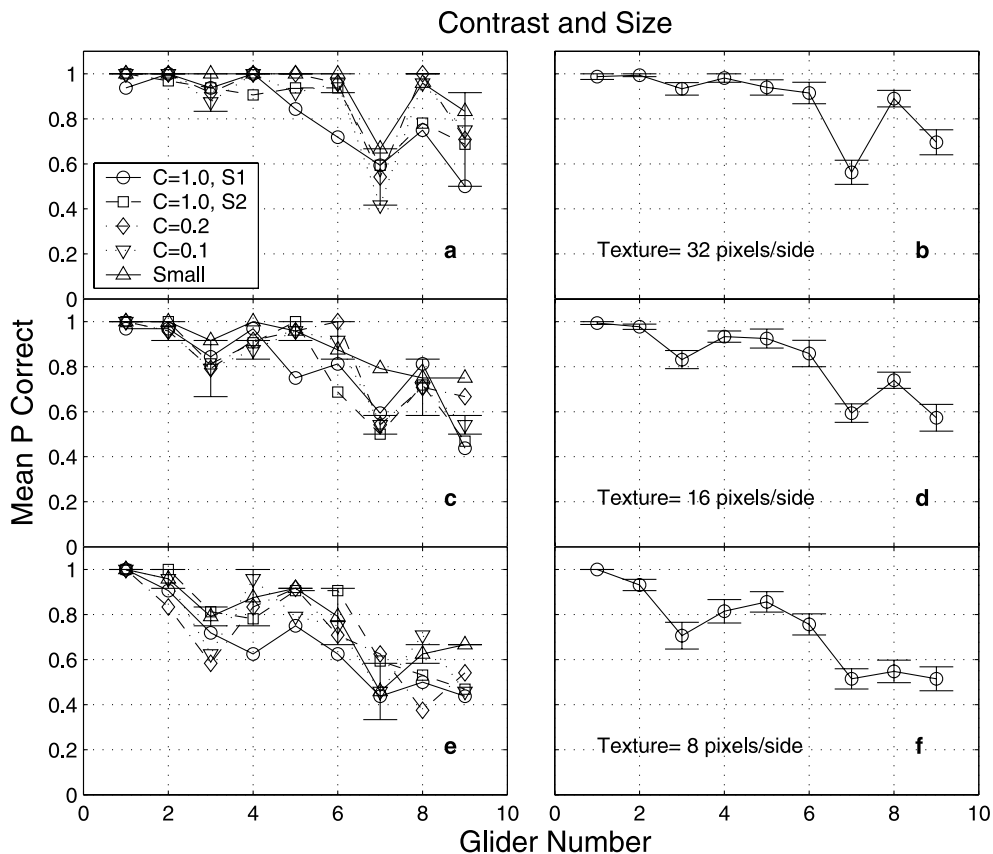


Fig. 7. Mean probability of correct discrimination for different contrasts and block pixel size (a, legend). Each curve in a, c, e is the average of data for the two authors and their ER, OR and EO discriminations. Conventions otherwise as in Fig. 5.

$i: \langle m_{r_i} \rangle$. That is to say for each mini-texture the corresponding mini-texture pixel values and receptive field weights were multiplied point-wise, and their sum was divided by the number of pixels. The calculation differed from a convolution in that we only considered adjacent, non-overlapping, mini-textures. We then calculated the Allan Variance in these receptive field outputs for $AV = \frac{1}{2} \sum (\langle m_{i+1} r_{i+1} \rangle - \langle m_{r_i} \rangle)^2 / N$. In fact the adjacent mini-textures for the whole sample texture were concatenated into one long row for this calculation so a few non-adjacent mini-textures were included into the calculation of AV. This was somewhat sloppy but the AV is a one-dimensional measure and the parent texture size was up to 256 pixels^2 , which for small mini-textures meant that only a small number of these edge effects occurred. Nevertheless, we will later introduce some two-dimensional variants of AV to resolve this problem and to address some other issues. We have included the one-dimensional AV data for comparative purposes. In the analysis that follows we took the square root of AV to give the Allan Deviation, AD.

A comparison of AD and the conventional standard deviation (STD) showed that, at least for receptive fields smaller than 8 pixels^2 , there is a significant

difference between these measures ($P < 0.01$). The data were based on twelve 256 pixel^2 textures made with 12 different random number seeds. Similar results were obtained for unoriented receptive fields and for receptive fields oriented at -45° and 45° (see Figs. 11 and 12). The total range of receptive field sizes for which AD and STD were calculated included receptive field sizes that were powers of two: 2 to 128 pixels/side, and also $\{3, 5, 6, 7, 10, 14, 15, 21\}$ pixels/side.

The input to the Discriminant analyses was 12 ADs computed for 12 textures for each mini-texture/receptive field size combination. There were thus 12 observations for each case, x_i , and we could increase the dimension of the observations and the discriminant models by increasing the number of receptive field sizes and types included in the model (Section 2). We computed Receiver Operator Curves (ROCs) for each texture type and model. Fig. 10 illustrates an ROC for the case of a model having four receptive fields, oriented and unoriented, each at two scales, 3×3 and 4×4 pixels (see inset Fig. 12), where the task was Odd vs. Random. The model was thus four-dimensional, each observation x_i having four AD measures. Twelve such observations were used to estimate

the coefficients for the LDA and QDA models summarised in Eqs. (2) and (3). The ordinate of Fig. 10 shows the Sensitivity (Sens) or the probability of correctly recognising an Odd texture as Odd based on the receptive field outputs. The Specificity (Spec) is the probability of reporting Random when the pat-

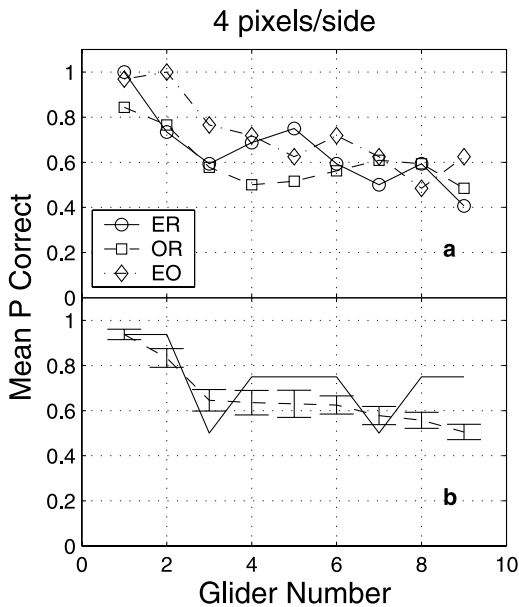


Fig. 8. Mean probability of correct discriminations for 4 pixel² textures. (a) Each curve is the average of two data sets collected during the first two repeats of the data shown in Fig. 6. (b) The average of the three curves of (a, dashed line) with SE. The solid line is a simple model based upon the number of mini-textures per texture (Section 3).

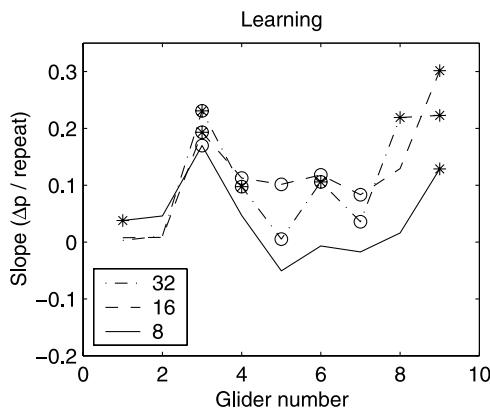


Fig. 9. The fitted slopes of the probability/trial over the five trials of Fig. 6. A positive slope indicates the increase in the probability correct (ΔP) across the five trials. The three lines represent outcomes for square textures having the side lengths shown in the legend. For each texture two models were fit, the simpler had two parameters: a mean probability and a slope, while the second model had separate means for the two subjects and a slope. In each case F -tests determined if the more complex, three parameter, model was justified at the $P < 0.05$ level. Circles indicate a significant slope ($P < 0.05$), * indicate the three parameter model was justified.

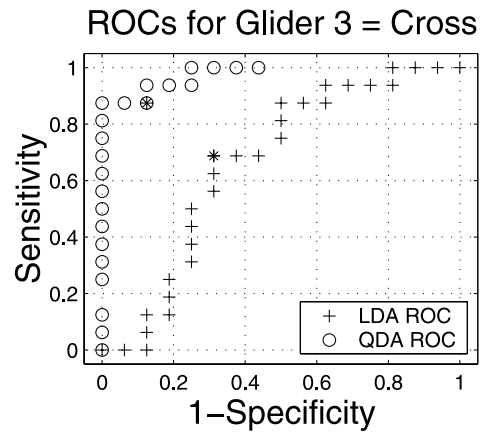


Fig. 10. Example of Receiver Operator Curves (ROCs) for linear (+, LDA) and quadratic (o, QDA) discriminant models. The particular case is for Cross textures and an OR comparison. The QDA curve is one of the nine ROCs computed to generate Fig. 12. Notice that as the probability of detecting Odd patterns from binary noise when presented with an Odd (Sensitivity) increases, the probability of falsely reporting a Random pattern as being Odd (1-Specificity) also increases. If there is no difference in the cost of falsely reporting Odd or Random then a good summary parameter for the ROC is the maximum simultaneously highest sensitivity and specificity (*s). Notice that the LDA model performs worse than the QDA model.

tern was Random. The abscissa is labelled 1-Specificity, this difference being otherwise known as the ‘false alarm’ or ‘false positive’ rate, i.e. the probability of reporting Odd when the texture was Random. Notice that to achieve higher sensitivities the system generates increasing false positive errors. This is the classical ROC case for a recognising a signal containing noise. If there is no difference in the cost of falsely reporting Odd or Rand a convenient way to summarise the ROC is to report the simultaneously highest sensitivity and specificity. These points are marked with * on the LDA and QDA ROCs of Fig. 10. We report these simultaneous sensitivity and specificities henceforth, or their average, since they may differ slightly for our discretely computed ROCs (Maddess et al., 1999b).

The outcome for QDA models containing receptive fields of different sizes, but all having the same orientation, is shown in Fig. 11. Notice that as the number of receptive field sizes is increased discrimination performance improves. Some models with oriented receptive field sizes around 12–16 pixels² produced uniformly good discrimination across all textures but in doing so did not mimic human performance (not shown). Nevertheless, even for models including five receptive field sizes, performance is less than perfect; however, some of the features of the human data are captured.

The upper panel of Fig. 11 displays output for un-oriented detectors. These models encompass ‘blob’ de-

tector models with various ranges of blob scale being incorporated. Inspection of the texture examples of Fig. 1 might suggest identification of blobs might be useful. Despite the QDA analysis attempting to find the optimum set of quadratic nonlinear interactions to discriminate the textures the Blob the models fail to mimic human performance. Notice also that human performance is nearly the same for Even and Odd textures even though blobs are generally less evident in the ODD patterns (Figs. 5–8).

Fig. 11 suggests an obvious way to improve performance: use several orientations, as many models of the human visual system do (Geisler & Hamilton,

1986; Caelli, Rentschler, & Scheidler, 1987; Watson, 1987). We could not build models with very large numbers of orientations as this would require a large number of observations in order to estimate the covariance matrices (Section 2). Employing a large number of observations to build a complex model would also not mimic our test conditions where relatively few targets of as few as 4×4 pixels were presented. We therefore examined models using a few oriented and unoriented receptive fields to span the orientation domain. Interestingly, models with relatively few receptive fields performed quite similarly to humans, even in the magnitude of the probability of

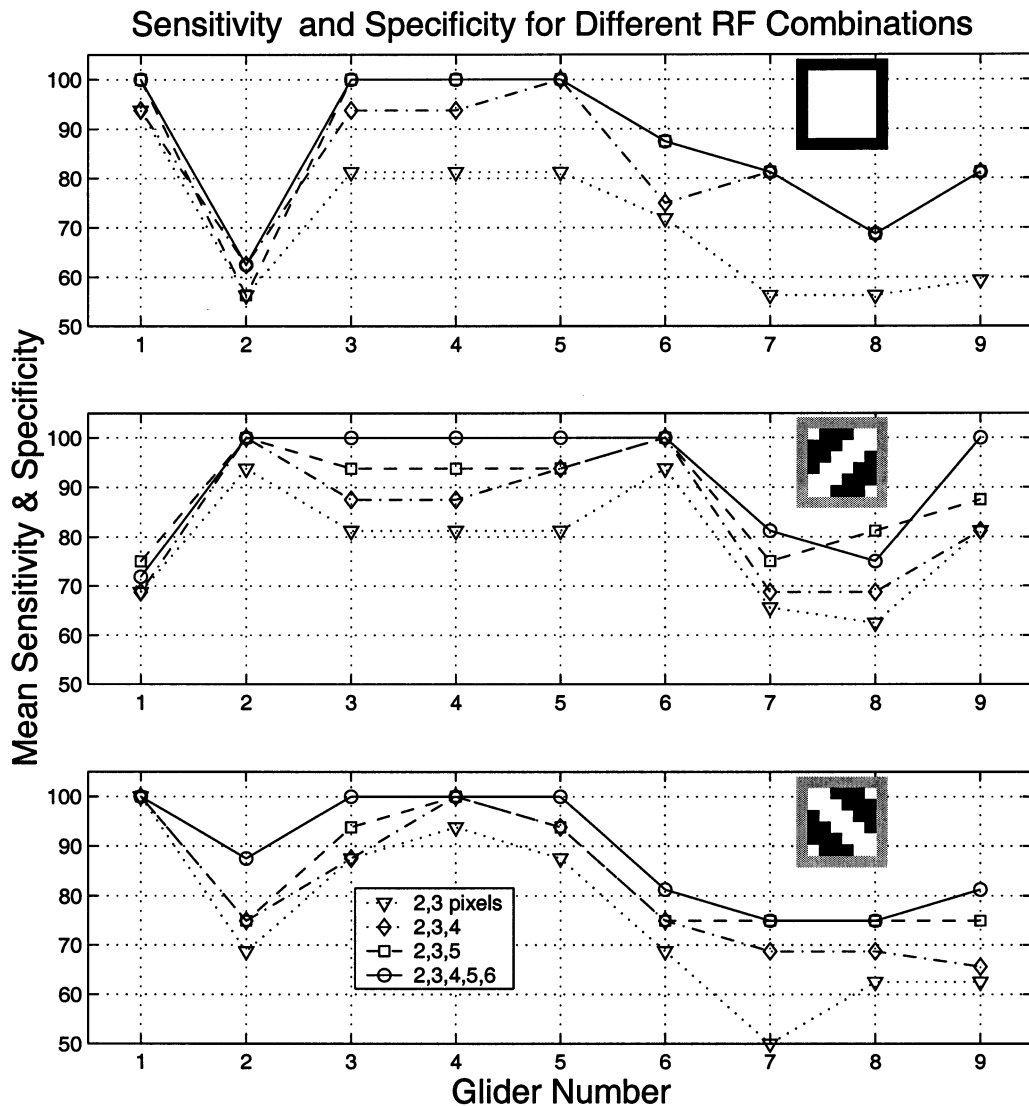


Fig. 11. Sensitivity and specificity for QDA models using combinations of receptive field (insets top right); and different sizes and numbers (legend). The simultaneously highest sensitivity and specificities are averaged together because, while they are theoretically the same, they occasionally differ due to the numerical procedure used to generate the ROCs (see Fig. 10). The example is for ER comparisons and one receptive field orientation: unoriented (top panel), 45° (middle panel), -45° (bottom) panel (e.g. insets). Discrimination improves as the number of receptive fields of different sizes increases. While the curves capture some of the qualities of the human psychometric functions they tend to have one or more major departures (especially for textures 1, 2 and 6), some receptive field orientations apparently being more useful than others for detecting particular textures.

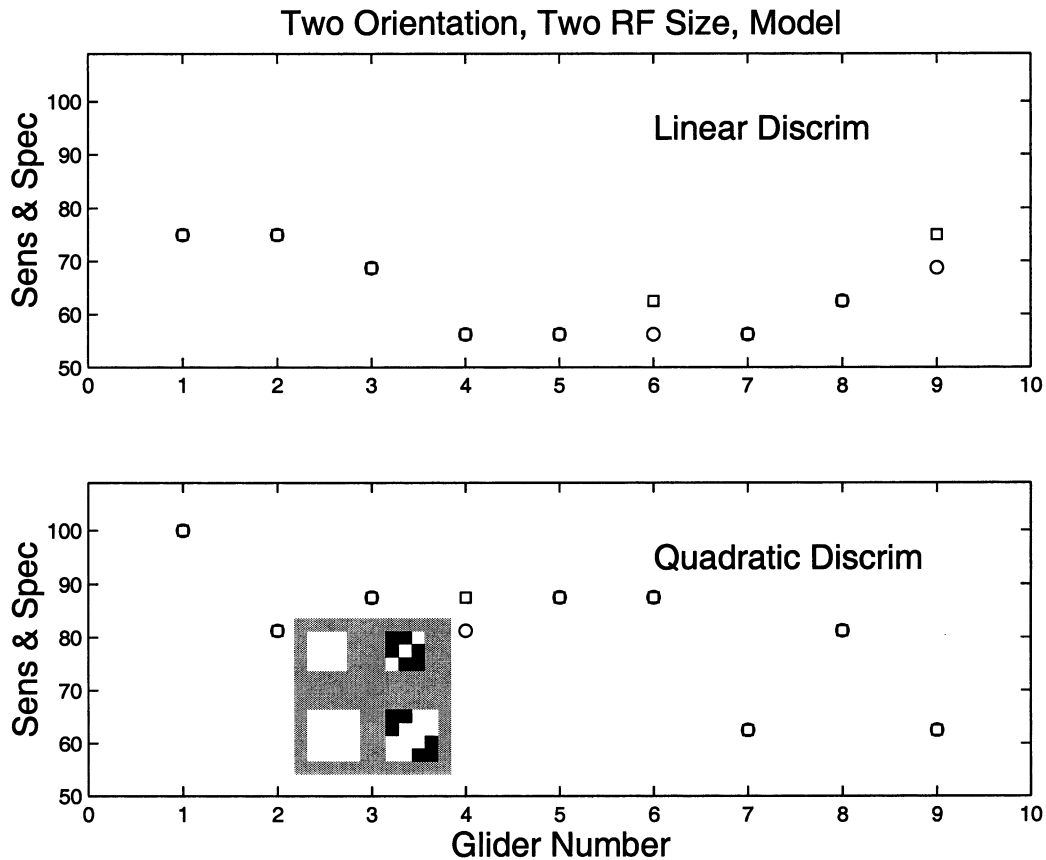


Fig. 12. Summary of a four receptive field model with mixed orientations (inset, lower). The ordinate is the simultaneously highest sensitivity (Sens, circles) and specificity (Spec, squares) (see Fig. 10). Upper: Linear discriminant models fail to get much above 75% correct in any case. The specific example is an OR comparison. Lower: The quadratic discriminant models show better overall performance except for textures 7 and 9, closely mimicking human performance (Figs. 5–8).

making a correct judgement (Fig. 12). Fig. 12 demonstrates another important outcome, also illustrated in Fig. 10, that *LDA models never performed well even with large numbers of receptive field types included in the models.*

Thus far we used the Allan Deviation as the input to the discriminant models. As mentioned this is not especially suited to two-dimensional textures. We therefore decided to examine some two-dimensional variants of the AD and also to compare all these models with the classical standard deviation in the receptive field outputs. To compute the standard deviation (SD) we simply took all the receptive field outputs from a given texture example and computed the standard deviation without regard to receptive field location. Notice that SD thus includes both short and long-range quadratic interactions.

Three local versions of the AD were also considered: an unoriented case (*UnO*) and two oriented cases (*Or1*, *Or2*). Here instead of simply taking the mean squared differences between receptive field outputs along a line of the parent texture we took instead *weighted 2D differences*, squared these and took

their mean. Thus, the difference in $\frac{1}{2}\sum (\langle m_{i+1} r_{i+1} \rangle - \langle m_{r_i} \rangle)^2/N$ is replaced by a local 2D differencing operation $D(\langle m_{r_i} \rangle)$ to give $\sum D(\langle m_{r_i} \rangle)^2/N$. The weights D used for the three variants were:

<i>UnO</i>	<i>Or1</i>	<i>Or2</i>
-1/8 -1/8 -1/8	-1/2 -1/2 1	1 -1/2 -1/2
-1/8 1 -1/8	-1/2 1 -1/2	-1/2 1 -01/2
-1/8 -1/8 -1/8	1 -1/2 -1/2	-1/2 -1/2 1

Thus, to compute each D , a set of nine spatially adjacent $\langle m_{r_i} \rangle$ were summed with the weights shown and the result was squared.

Since there appeared to be some similarity between the human data and the model outputs (Figs. 5–7 and 12) we next attempted to quantitatively compare human data with the outputs from the various models. We first did this by taking the psychometric functions averaged across five subjects for ER, OR and EO comparisons of 32 pixel² patterns (Fig. 5) and we regressed these against means of the simultaneously

maximum sensitivities and specificities obtained from versions of QDA models having different variance models. The regression took two forms, fitting a mean effect and a scaling, or only a scaling. The simpler single-parameter scaling operation proved the best in terms of mean square errors and so we report that here, although the results were similar for the two parameter regression. We applied two further variations: fitting data and model outputs for all nine gliders, or only data and model output for gliders 3–9. We will refer to these two cases as G_{all} and G_{39} . The G_{39} method eliminated the possible effects of saturation seen for gliders 1 and 2.

Fig. 13 shows average QDA model output for seven sets of 60 pixel² Even and Random input textures (circles, error bars) and the corresponding best fitting scaled psychometric functions for the case for ER comparisons (solid lines). In this case the model

using the global variance (Var) in receptive field outputs, Fig. 13 e and f provides data most closely mimicking the psychometric data for both G_{all} and G_{39} . The model data shown in the left and right columns differ in the tilt of the two oriented receptive fields (titles, caption) which were otherwise as shown in the inset Fig. 12. Each panel of Fig. 13 contains a legend describing the variance model, the t -statistic for the regression, and the resulting scaling factor required for the best match between model and human data. The left column shows fitted psychometric functions when data for all textures are compared (G_{all}), while the right column shows the outcome when only data for textures 3–9 are included in the regressions (G_{39}). Neither, G_{all} or G_{39} models produced significantly larger t -statistics on average. Of the 24 cases examined (G_{all} and G_{39} , using ER, OR, EO and Ave comparisons, for sixty 120 and 240 pixel² input textures)

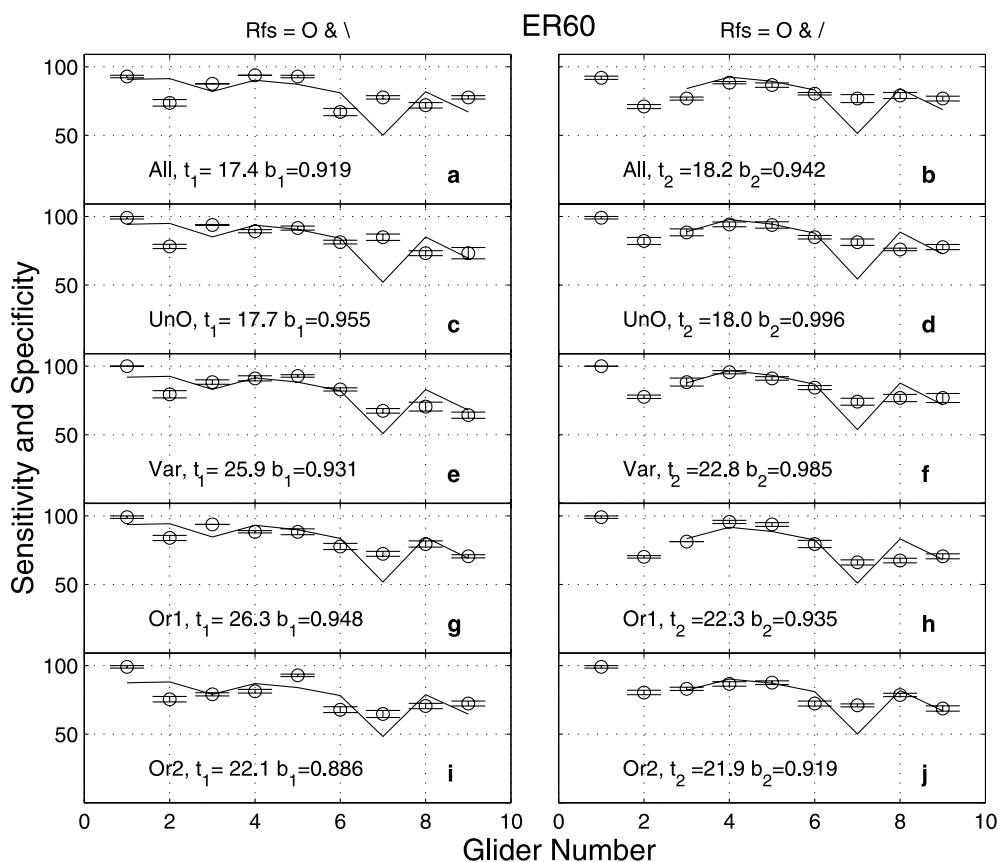


Fig. 13. Comparison of QDA output and human data. All QDA models were like that for Fig. 12 using 3×3 and 4×4 pixel receptive fields: two oriented and two unoriented. In this particular example all panels are ER comparisons and the solid curves are scaled versions of the 32 pixel² psychometric functions for ER comparisons for five subjects from Fig. 5a. The left column (a, c, e, g, i) is for models where the receptive fields were unoriented or -45° and where the regression included data for textures 1–9. The right column (b, d, f, h, j) is for models with receptive fields that were unoriented or 45° , and where the regression included only model and human data from textures 3 to 9. The five rows of panels summarise results for QDA models where different variance models were used. From top to bottom the models were: all Allan Deviation, UnO unoriented 2D Allan Deviation, Var global Standard Deviation, Or1 -45° oriented 2D Allan Deviation, Or2 45° oriented 2D Allan Deviation. Each case the t -statistic is reported for a one parameter regression model providing a best scaling of the psychometric function for to the particular model output. The scale value, b_i is also given. All the scale values are close to 1. The t and b values in both columns are for the right column cases only.

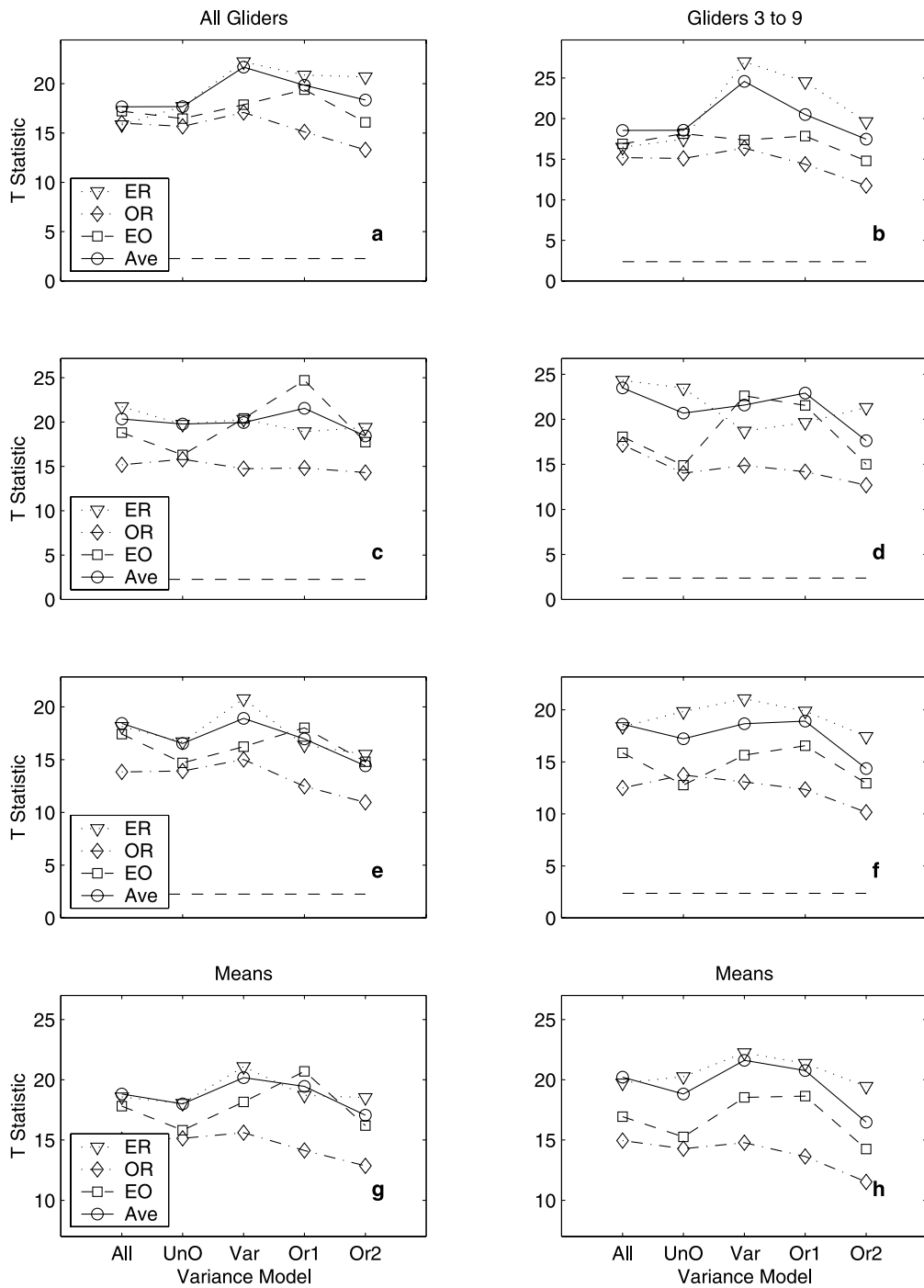


Fig. 14. The process illustrated in Fig. 13 was repeated for ER, OR and OE comparisons (legends) and for three texture sizes, 60 (a, b), 120 (c, d), and 240 pixels² (e, f). Seven examples of each texture type were generated for each texture size using different random number seeds. In this way the five variance models (abscissa labels defined in text) were compared for smaller to larger mini-texture data sample sizes. Larger training sets did not perform better. Each panel shows the *t* values obtained for the best scaling of the psychophysical data for different comparisons. In the case of the curves labelled *Ave* the fits were between the averaged psychometric function and the average of the model discriminant functions for ER, OR and EO. The horizontal dashed line indicates the *t* value for a nonsignificant regression. The bottom row (g, h) represents the means across the three texture sizes. The left column of panels (a, c, e, g) are *t* values when regressing data for all nine textures, while the right column (b, d, f, h) is for regressing model and data for textures 3–9 only. Except for g, h (see Fig. 15) the SE ($N = 7$) are about the size of the symbols.

the scaling factors were only significantly different than 1 in one case: EO for 240 pixel² inputs for the case of all nine inputs, where the scaling was 0.86 ± 0.014 SE ($P = 0.011$). Fig. 14 summarises the outcomes for all 24 cases. We also redid this analysis regressing against the psychometric functions obtained from five subjects for the 16 pixel² textures (Fig. 5c). This produced very

similar results as did using psychometric functions from 8 pixel² textures (although the scaling factors became larger).

We repeated the analysis of Fig. 14, where the fits were based on data of Fig. 5a, using both the psychometric functions obtained from the five repeats by the authors (Fig. 6a), and for the combined psychometric

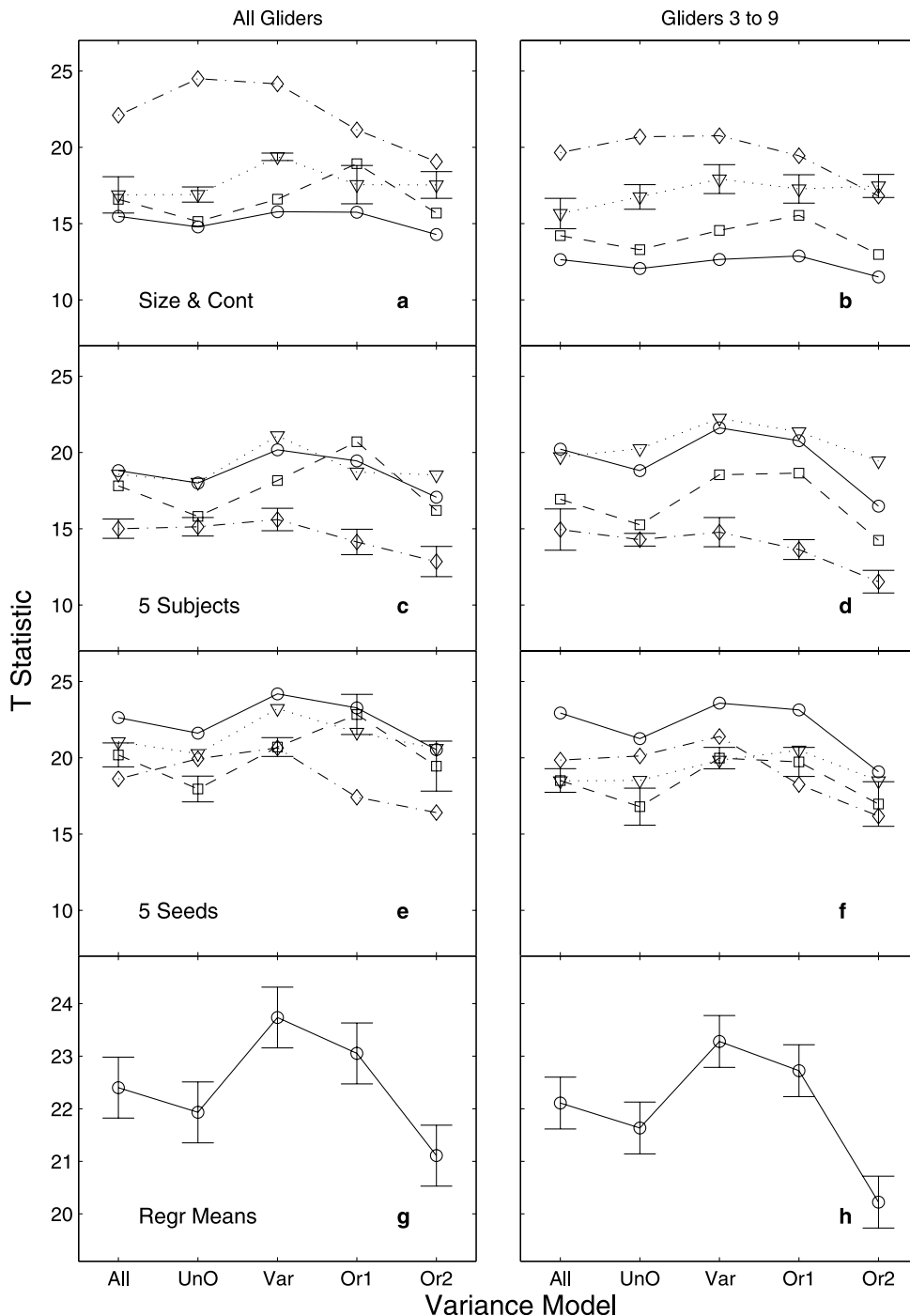


Fig. 15. The modelling process summarised in Figs. 13 and 14 was repeated using the psychometric functions derived from the data sets illustrated in Figs. 5–7. As in Fig. 14 columns of panels represent regressing data for all nine gliders (a, c, e) and only gliders 3–9 (b, d, f). Each panel is a mean for three texture sizes as in Fig. 14g, h, which are reproduced as c, d here. The mean shape of the curves in a to f as determined by a multiple regression model and are shown in g, h. One set representative error bars (SE, $N = 3$) for each panel are shown.

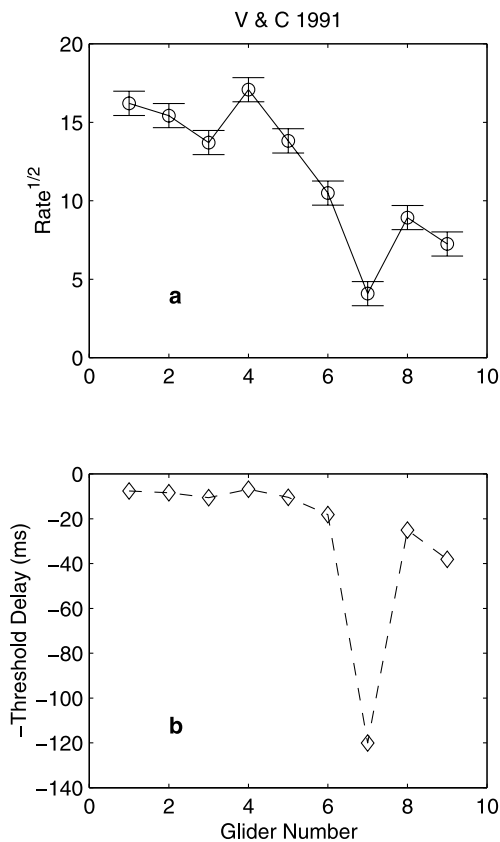


Fig. 16. (a) The mean square roots of the *rates* tabulated by Victor and Conte (1991). One per rate is a measure of the delay in time to threshold (75% performance) for a hypothetical set of neurons. Larger rates thus indicate the degree of local decorrelation that could be introduced into Even versions of the textures used before discrimination from random textures failed. (b) The plot shows $0-1/\text{rate}$, where rate is derived from the fitted values shown in (a). The vertical inversion was done to have downward displacement indicate poorer performance.

functions obtained for different contrasts and pixel sizes (Fig. 7a). The mean *t*-statistics are summarised in Fig. 15. If we want to examine the shape of the average functions in Fig. 15 there is a problem in that different cases clearly have different mean *t*-statistics. A reasonable approach therefore is to fit a regression model estimating coefficients across the five variance models, providing offsets for each case. In this way we extract the average function shape without injecting variance due to the different means for different cases. Overall the fit of these multiple regression models was good for both the G_{all} ($F = 21.6$, $df = 16.44$, $P < 0.0000$, $r^2 = 0.88$) and G_{39} ($F = 39.9$, $df = 16.44$, $P < 0.0000$, $r^2 = 0.93$) cases. The resulting regressed means are shown in Fig. 15g, h.

We further examined models where a single coefficient (mean) was used for variance models Var and OR1 and these were not significantly ($P = 0.16$) different to the case of separate means both G_{all} and G_{39} . Thus, the Var and OR1 variance models are about

equally good matches to the psychometric data. All simpler models produced significantly poorer fits. For example, using a single mean for All, Var and OR1, but separate means for UnO and Or2, was a significantly poorer model than that combining only Var and OR1 ($P = 0.017$ and 0.012 for the G_{all} and G_{39} cases). Thus, the most parsimonious regression model is one with a combined mean for Var and OR1 and different means for the other variance measures.

4. Discussion

A considerable volume of research examining the responses of single striate cortical neurons has concentrated on aspects of their spatial frequency and orientation tuning. The Fourier transform of the power spectrum of the spatial frequency tuning is the spatial autocorrelation function. Therefore, these studies have in effect been concentrating on the two-point correlation properties of these cells. More recent work (Purpura et al., 1994), using isotrigrion stimuli, has shown that almost all cells within primate V1 encode higher order correlations. Three point (third order) correlations, and higher order, inform us about spatial phase relationships, critical to the recovery of salient image components like edges. The results from V1 are supported by PET and fMRI data showing cortical areas apparently dedicated to the higher order correlation properties of visual stimuli (Beason-Held et al., 1998a,b; Beason-Held et al., 2000). Given the potential interest in isotrigrion stimuli then we thought it would be useful to quantify for the first time the complete range of ER, OR and EO discriminations for the isotrigrion stimuli used in psychophysical and VEP studies to date (Victor & Conte, 1991). We also manipulated stimulus extent, contrast and pixel size for all these stimuli (Figs. 5–8). Given the quite local analysis of cells in V1 we also sought to quantify the number and frequency of mini-textures within the 18 isotrigrion stimuli examined (Tables 1–3 and A1). These findings now permit studies that compare isotrigrion textures sharing no, or some number, of mini-textures. Our data also reveal that discrimination of some textures shows significant long-term learning effects (Fig. 9).

In a VEP study using Even textures of the Box type Victor and Conte (1989) found that spatial interactions critical to making ER discriminations proceed on scales proportional to pixel block size, at least for pixel blocks ranging from of $4'$ to $16'$ square, where this critical interaction distance is about 3–4 pixels. We confirm that psychometric discrimination functions for all nine glider types differ little for block pixel sizes $14.5'$ and $58'$ square (Figs. 5 and 6 with Fig. 7), and that this holds for OR and EO comparisons also. A comparative VEP and psychophysical study (Victor & Conte, 1991)

also examined Even vs. Random comparisons for the nine glider types employed here, but where the sort-range correlations of the Even textures was manipulated. They characterised their data by fitting a model based on the rate of activation of hypothetical neural units (Victor & Conte, 1990). In their model the amount of decorrelation of Even textures required for subjects to achieve 75% discrimination from Random binary textures is proportional to $1/\text{rate}$, a sort of delay to threshold. They tabulated their fitted rates for six subjects, and nine Even (and one Odd) textures. Since the subjects had quite different mean rates we have fitted a multiple regression model similar to that for Fig. 15g, h. Significantly different subject means were found and the overall model ($F = 34.0$, $df = 14.40$, $P < 0.0000$) accounted for 91.7% of the variance. To provide reasonably Gaussian distributed data we fitted the square root of the rates (Fig. 16a), and later squared these values to produce Fig. 16b. Both figures show similarities to our measured ER discrimination functions (Figs. 5–8), particularly in having dips at glider/texture numbers 3 (Cross), 7 (Wye) and 9 (El). The similarity is heartening because while both studies used memory based comparisons Victor and Conte used shorter presentation times (50 ms) and post-presentation masking. The difference in methodology appears to have made little difference to the outcome.

In the analysis summarised in Figs. 13–15 we directly compared the probability of correct discrimination by our subjects with the mean simultaneously highest sensitivity and specificity of the QDA models. There is no a priori reason why these probabilities should be the same size, nevertheless the required scaling factors differed from 1.0 in only 1 of the 60 cases examined for comparison with psychophysical data for 32 pixel² textures. As noted in Section 3 the reason for using the simultaneously highest sensitivity and specificity is that it represents the best that a model governed by a ROC can do when the penalty for incorrect decisions is the same for either type of test pattern, as was the case for our subjects. Thus, the fact that the scaling factors differed little from 1.0, indicated that humans behaved like an ideal observer using a discrimination process based on measures related to those employed in our models. R ath and Morfill (1997) also used ROC analysis and a similar criterion to assess their texture discrimination model.

Models of texture segregation have concentrated on identifying the basic mechanisms that must underlie this ability (Beck et al., 1987; Sutter et al., 1989; Landy & Bergen, 1991; Graham et al., 1992; Graham & Sutter, 1996, 2000). The present study seeks to compliment these analyses by introducing both isotrigon textures and formal statistical discriminant

models. Part of the concept behind the discriminant models is to compare quadratic and linear models given a fairly limited number of samples, as the human subjects had in our tests. A secondary objective was to see if either type of discriminant model would show behaviour that was anything like that of human subjects.

The host of data indicating initial processing of textures by neurons with small, linear, oriented receptive fields, suggested that examining small texture domains, mini-textures, might be sensible. Also, linear summation by these receptive fields would clearly reduce the alphabet of mini-textures available for discrimination. Indeed, a simple model indicated that discrimination is not directly related to number of mini-textures available (Fig. 8b). Nevertheless, the number of mini-textures unique to given texture types was not a very poor predictor of discrimination either, suggesting that some modification of mini-texture number, as spatial summation would afford, determined discrimination performance.

While it is clear that linear summation acts to reduce the number of independent inputs possible from a given texture class, it is equally clear that that *non-linear interactions can increase the alphabet size*. For example, if one had two independent linear receptive field outputs, a and b , for two (or more) types of mini-texture, then $(a \pm b)^2$ leads to response terms in a^2 , ab and b^2 , three independent measures. If we consider products of linear combinations of a and b up to order d , then dimensionality of the *feature space* into which the discrimination problem is cast grows as 2^d , and N^d , for N inputs (Sch olkopf, Smola, & M uller, 1998) (see also, Maddess, Davey, & Yang, 1999a). Notice that the Allan Variance measure we selected has the form $(a - b)^2$, being based on the square of local differences of mean receptive field output in response to mini-texture input. As outlined in Section 2, the Allan Variance and its derivatives may have some utility compared to traditional variance measures, and is related to wavelet variance (Howe & Percival, 1995).

Other authors have considered the dimensionality of the feature space in which textures are discriminated. Methods for measuring the feature space dimension for compound wavelet patterns have been derived (J uttner & Rentschler, 1996, 2000). The methods have been extended to following how the dimensionality changes with learning (Rentschler, J uttner, & Caelli, 1994). The method begs the question as to whether isotrigon patterns could not be used in a similar way. One approach would be to define a space based on the commonality of mini-textures between isotrigon texture classes (Table 2). Thus, textures sharing very few mini-textures would be nearly orthogonal while those with many common mini-textures

tures would be largely collinear in such a feature space.

None of the linear discriminant models we made gave good discrimination (Figs. 10 and 12). This is not entirely surprising because in order to discriminate an ensemble of isotrigon textures from another group by definition requires examination of fourth order correlations (Victor, 1994). The linear comparison of variances afforded by LDA is formally second order. By contrast, the quadratic discrimination models (QDA) we examined performed more like humans, even in the detailed shape and magnitude of discrimination the discrimination functions (Figs. 12 and 13). Presumably the quadratic models work because, by being based on quadratic interaction between variance measures (Eq. (3)), they are formally *fourth order*. A necessary condition for good performance was that the initial linear spatial filtering had to be done by receptive fields that

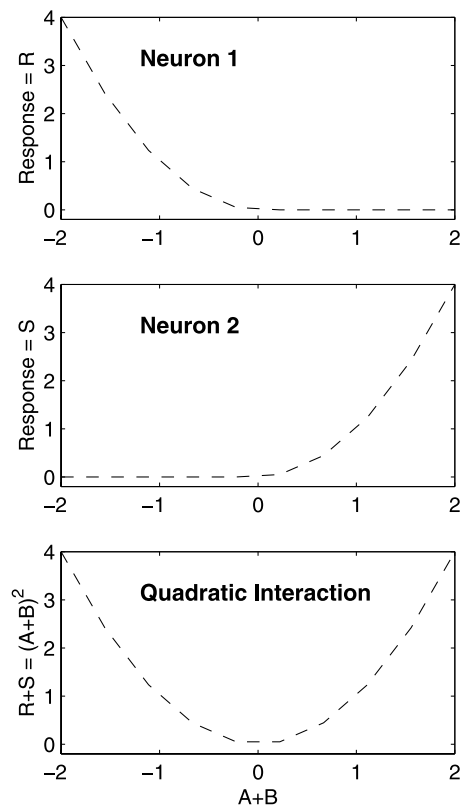


Fig. 17. A physiologically plausible model for quadratic interactions using rectification and summation. Top: Neuron 1 having a *soft* (quadratic-like) half-wave rectified response to the summed input from 2 pixels A and B . The summation $A+B$ could occur by both pixels falling within a positively weighted receptive field. Middle: Neuron 2 responding similarly but to positive excursions of $A+B$. Bottom: A third neuron sums the outputs, R and S , from the first two neurons. Note that due to the soft rectification $R+S \approx (A+B)^2$. Differences described in the text, like $A-B$, can be computed by receptive fields like the partial derivative (d/dx) of a 2D Gaussian, with A and B placed in the positive and negative lobes, respectively, providing $(A-B)^2$. A subsequent difference between the two squares, $(A+B)^2 - (A-B)^2$, gives $4AB$. Cascading two similar processes can provide pure fourth order correlations.

spanned the orientation domain and which operate at (at least) a few, small, scales (Figs. 12 and 13).

Victor and Conte (1989) point out that operation $(a+b+b+d)^4$, where $a-d$ are receptive field outputs, would yield products in $abcd$, i.e. four point correlations. As indicated by those authors, however, the other resulting products, a^2bd etc. would make the $abcd$ term relatively small, and a tiny fraction of any neuronal response. Nevertheless, the above discussion suggests that we might have obtained similar performance by raising our local differences to the fourth power: $(\langle m_{i+1} r_{i+1} \rangle - \langle m_i r_i \rangle)^4$, and then constructing linear discriminant models on that output. Psychophysical studies of putative complex channels in texture segregation indicate exponents between 3 and 4 are involved (Graham & Sutter, 1998), but whether these are generated by a single neural mechanism or represent cascaded, less steeply accelerating, response nonlinearities is unclear.

A possible advantage of our formulation with two levels of quadratic interaction is that if adaptation is introduced at each stage (as for example, in taking the mean rather than the summed receptive field output) then such a neural system would be *less likely to saturate*. Adaptation is a well-known feature of striate cortical neurons (Maddess, McCourt, Blakeslee, & Cunningham, 1988; Carandini & Heeger, 1994; Carandini, Heeger, & Movshon, 1997).

Physiologically feasible models exist for obtaining squares of linear combinations of inputs and have been used to construct physiologically plausible versions of the Reichardt and Motion Energy models using only rectification and summation (Emerson et al., 1992). If one removes the delay stage from these models measures like the Allan Variance can be obtained (see below). Moreover, these models get rid of unwanted products (as occurs in the case of $(a+b+c+d)^4$ above), and so there may be less need for gain control to prevent saturation. So, for 2 pixels a, b two squares are computed (Fig. 17) and differenced: $(a+b)^2 - (a-b)^2 = 4ab$, thus eliminating the self quadratic terms in a^2 and b^2 . Cascading this type of operation, and introducing two other pixels c and d , we obtain: $(ab+cd)^2 - (ab-cd)^2 = 4abcd$, a pure four point correlation without other products to cause saturation problems for any neuron. If ab and cd are replaced with averages of similar products from nearby locations, $\langle a_i b_i \rangle$ and $\langle c_i d_i \rangle$, and a to d are differences from mean pixels outputs (contrasts) then we essentially have the models used here that are based on quadratic interactions between local variances. The present models, being cascades of two quadratic stages of processing, also resemble some models for non-Fourier motion detection (Zanker, 1996).

While the models presented are physiologically plausible we have to concede that it is difficult to distinguish high and low level processes and the present work only

points out the necessary order of nonlinearity and a correlation, albeit good, between human performance with isotrigran textures. Rubenstein and Sagi (1990) using a method involving means and variances of wavelet energies reproduced the texture asymmetry results of Gurnsey and Browse (1987) with non-isodipole stimuli.

The models of texture discrimination of Malik and Perona (1990) are of particular interest because they recognise formally that multiple levels of nonlinear interactions are required to discriminate classes of textures that have equal lower-level correlations. The textures they considered are different than those used here, and the comparison with human performance was less direct, but the similarities make comparison of our respective models important. At the initial input level our models are similar in having both oriented and unoriented spatial filters. Then Malik and Perona introduced two nonlinear stages of processing, both involving the use of taking the maximum value (Max) between several (spatially weighted) inputs at each particular level. At the top level a 'texture gradient' is computed through an operation that takes differences between adjacent elements, through the use of odd receptive field weighting functions, and then applying the Max operation again. The model could thus be described as comprising the stages: *filter with oriented and unoriented operators, nonlinear interaction between units (Max) with local differences (akin to our Allan Variance), nonlinear interaction between units (Max)*. Thus, if the two stages of Max operation could in some sense be shown to be equivalent to our quadratic interactions then the models could be said to be similar.

The objective of the Malik and Perone in using the Max function was to minimise contributions from weakly contributing, and hence less salient, neural elements. We could model this reasonably well by thinking of the outputs of the first stage of Max operations, F , as taking the values $\{0, 1\}$, 0 being frequently realised in their model and 1 denoting a salient response. Similarly, the second stage of Max operations, S , on a set of these outputs effectively maps the first set of $\{0, 1\}$ patterns, F , to S under a mapping or rule r , $r(F\{0, 1\}) \Rightarrow S\{0, 1\}$. Different textures producing different collections of mappings onto the second layer S . Such transformations are similar to the rules for cellular automata and the set of all such mappings or rules can be expressed in a matrix form that permits us to see the relationship between our models.

In the model of Malik and Perone the interactions were fairly short range. If we have mappings as described that are dependent upon the activity of three neighbours $\{a, b, c\}$ then for the two level $\{0, 1\}$ case there are 2^8 possible mappings. It can be shown

(Ankiewicz & Nagai, in press, Nagai, Maddess, & Ankiewicz, 2001) that for a function $v(a, b, c) = (1, a, b, c, ab, ac, bc, abc)$ there exists a discrete function f , and a row vector of coefficients x , such that the $f = vx^T$ (T denoting the transpose). Also, a matrix S can be formed whose rows are every combination of v for a, b and c taking the values $\{0, 1\}$, such that all possible rules r , are given by $Sx^T = r$, the coefficients x being given by $x = S^{-1}r^T$ (-1 denoting the matrix inverse). The important point here is that *all the possible three neighbour mappings* $r(F_i\{0, 1\}, F_j\{0, 1\}, F_k\{0, 1\}) = S\{0, 1\}$ are described by f , which has the form $f = x_1 + x_2a + x_3b + x_4c + x_5ab + x_6ac + x_7bc + x_8abc$. Thus, if we permit ourselves to characterise the cascading of two levels of Max operations across three inputs (or sets of three inputs) as the mappings or rules $r(F_i\{0, 1\}, F_j\{0, 1\}, F_k\{0, 1\}) = S\{0, 1\}$ for three neighbours then what we are saying is that the interactions between the levels are decomposable into a set of (frequently) quadratic interactions between the first stage inputs a, b, c , i.e. the response for many mappings contains terms like $x_5ab + x_6ac + x_7bc$. Interactions between more neighbours, say $\{a, b, c, d, e\}$, leads to similar discrete functions (Ankiewicz & Nagai, 2001; Nagai et al., 2001), and so too responses, containing higher order products like $ace, adc, abcde$. Armed with this information we can now see the model of Malik and Perone can be sketched as having the stages: *filter with oriented and unoriented operators, sums of quadratic (or higher order) interactions with local differences, sums of quadratic (or higher order) interactions*. This is thus very like the models proposed in the present paper. Both models share features of others used for non-isodipole textures (Laws, 1980; Rubenstein & Sagi, 1990; R ath & Morfill, 1997).

Part of the reason for introducing the 2D versions of the Allan Variance used here was that previous work on discrimination isotrigran textures indicated that, for textures consisting of pixel blocks greater than $4'$ on a side, most of the important spatial interactions (at least for ER comparisons) took place over a range of about 3 pixels (Victor & Conte, 1989). Our unoriented and oriented Allan Deviations (UnO , $OR1$, $OR2$), in combining information arising from mini-textures as large as 4 pixels², include interactions out to about 8 pixels from a central pixel. Nevertheless, the global variance measure, Var , provided as good a model as $OR1$, and better than UnO or All . This suggests long-range correlations may be more important than was thought. At the same time the case for accepting the $OR1$ model is supported by texture segregation models where both input and output stages are oriented (Landy & Bergen, 1991; Graham et al., 1992; Graham & Sutter, 1996, 1998, 2000). A curious feature of the present models was

that *OR1* was better than *OR2* whether or not the orientations of the input receptive fields and the subsequent differencing operator were parallel or orthogonal. Apparently the orientation of the latter operator was the important feature. Some recent texture segregation studies include mixtures of linear and nonlinear inputs to the (undefined) decision process, and or interactions between these units (Graham & Sutter, 1998, 2000). Our analysis says nothing about such interactions but perhaps the discrimination of the Triangle texture might be facilitated by such a mechanism. Of all the textures tested it is only isodipole with random textures. Thus, the fourth order mechanisms described above are not required to discriminate Triangle textures from random textures.

A proposed model for ER discriminations (Victor & Conte, 1991) comprised oriented rectifying subunits followed by a strong threshold. A key feature of this model is the summation of six or more of these rectifying units to make a rather elongated receptive field, which would have a very narrow orientation tuning. The model was tested only on ER comparisons for the standard Box glider textures. In our case the use of larger oriented input receptive fields sometimes yielded good performance, but discrimination by these models was quite uniform across the different texture types, unlike human performance. Very elongated receptive fields are quite rare in striate cortex, although elongated disparity units have been reported (Ohzawa, DeAngelis, & Freeman, 1997). Highly orientation tuned and rectifying neurons are reported in cat area 21a (Dreher, Michalski, Ho, Lee, & Burke, 1993), however, and also in bees (Yang & Maddess, 1997), which have been shown capable of discriminating isotrigon textures (Maddess et al., 1999a).

Whether our actual neural machinery relies upon a single rapidly accelerating nonlinearity (Graham & Sutter, 1998) or a cascade of nonlinearities as used in the present paper and elsewhere (Malik & Perona, 1990; Victor & Conte, 1991), it seems clear that consideration of higher order image correlations is necessary for understanding image structure. This information is encoded by many striate cortical cells (Purpura et al., 1994). As pointed out above cascade models may have advantages from the point of view of reducing saturation problems. Certainly, nonlinear spatial interactions seem to be related to responses to contours (Polat, Mizobe, Pettet, Kasamatsu, & Norcia, 1998; Chen, Kasamatsu, Polat, & Norcia, 2001). More generally, a number of sophisticated methods for separation of signals, including Independent Component Analysis and Nonlinear Principal Component Analysis, have all been shown to rely on fourth order correlations (Lee, Girolami, Bell, & Sejnowski, 2000) to minimise mutual information in order to achieve segregation. It would be surprising if our brains did

not use related methods to solve signal segregation and discrimination problems.

Appendix A

If we have a $N \times M$ random binary texture $R(N, M)$ having an equal probability of its two states, say $\{-1, 1\}$ or $\{0, 1\}$, then the possible number of different $N \times M$ textures $N(R(N, M)) = 2^{NM}$. In the case of the Box isotrigon textures (Odd or Even) the application of the Box glider, to a matrix of random $\{-1, 1\}$ elements means that the resultant textures are deterministic because the state of 3 glider pixels determines the state of the fourth (Section 2). For the Box glider we can summarise this by saying that the state $S(i+1, j+1)$ is a function of the three other pixels determined by the glider,

$$S(i+1, j+1) = F(S(i, j), S(i+1, j), S(i, j+1)).$$

In this case the resultant deterministic texture $D(N, M)$ will have a number of possible states $N(D(N, M)) = 2^{N+M-1}$. This can be understood as follows. Assign the pixels of the first row and column randomly. We refer to these as *random pixels*. The other pixels are all assigned by the recursion rule determined by the Box glider. These are thus described as *deterministic pixels*. For example, if we represent the Box glider (Fig. 1) as,

$$\begin{array}{ccc} * & * & n \\ * & d & n \\ n & n & n \end{array}$$

where the central pixel d is determined by the three * pixel values. The null pixels, n , contribute nothing to d . Then we obtain a texture that can be shown as:

$$\begin{array}{cccccc} & 1 & 2 & 3 & 4 & \dots & n \\ 1 & \# & \# & \# & \# & \dots & \# \\ 2 & \# & x & x & x & \dots & x \\ 3 & \# & x & x & x & \dots & x \\ \vdots & \vdots & \vdots & \vdots & \vdots & \ddots & \vdots \\ m & \# & x & x & x & \dots & x \end{array},$$

where $\#$'s denote random boundary pixels and x 's denote deterministic pixels determined by the glider. Since the random pixels ($\#$) take two values such as $\{-1, 1\}$ or $\{0, 1\}$, while the deterministic pixels are uniquely determined by the boundary random pixels, *thus all possible generated textures are completely determined by the random boundary pixels*. Different textures are obtained by a different initial random pixel assignments. The number of random pixels (in the first row and column) is $n+m-1$ because the top left corner (1, 1) is a degenerate pixel for counting. Hence, we know that the possible number of $N \times M$

Table A1

Glider	Glider rule	$N(D(N, M))$	$N_{3 \times 3}$
Box	$S(i+1, j+1) = F(S(i, j), S(i+1, j), S(i, j+1))$	2^{N+M-1}	$2^5 = 32$
Triangle	$S(i+1, j+1) = F(S(i+1, j), S(i, j+1))$	2^{N+M-1}	$2^5 = 32$
Cross	$S(i+1, j+2) = F(S(i, j+1), S(i+1, j), S(i+2, j+1))$	$2^{2N+2M-4}$	$2^8 = 256$
Zigzag	$S(i+1, j+1) = F(S(i+1, j), S(i+2, j), S(i, j+1))$	2^{N+2M-2}	$2^7 = 128$
Oblong	$S(i+2, j+1) = F(S(i, j), S(i+2, j), S(i, j+1))$	2^{N+2M-2}	$2^7 = 128$
Tee	$S(i+2, j+1) = F(S(i+1, j), S(i, j+1), S(i+1, j+1))$	2^{N+2M-2}	$2^7 = 128$
Wye	$S(i+2, j+2) = F(S(i+1, j), S(i, j+1), S(i+1, j+1))$	$2^{2N+2M-4}$	$2^8 = 256$
Foot	$S(i+2, j+1) = F(S(i+1, j), S(i+2, j), S(i, j+1))$	2^{N+2M-2}	$2^7 = 128$
El	$S(i+2, j+1) = F(S(i, j), S(i+1, j), S(i+2, j))$	2^{N+2M-2}	$2^7 = 128$

Even/Odd textures for the Box glider is 2^{n+m-1} . Notice that the value 2 comes from the fact that each random pixel takes one of two possible values, and the state of any random pixel is determined independently to every other random pixel.

For other glider textures, we count the possible number of textures in the same way except that we often have to assign more random pixels than just the first row and column. Notice that the same rules apply to every mini-texture of any larger parent texture, hence 3×3 mini-textures produced by the standard glider will have $2^{3+3-1} = 32$ possible states. As far as the standard Box textures are concerned this means that as N and M grow larger the possible textures represent a decreasingly small proportion of the possible random binary textures since $N(D(N, M)) / N(R(N, M)) = 2^{N+M-1} / 2^{NM} = 1/2^{(N-1)(M-1)}$. For other gliders we can ascertain the $N(D(N, M))$ by inspection of the glider rule and counting the minimum number of necessary random pixels. The glider rules and the resultant number of deterministic textures for a $N \times M$ pixel texture are summarised in Table A1.

References

- Allan, D. W. (1966). Statistics of atomic frequency standard. *Proceedings of IEEE*, 54, 221–231.
- Ankiewicz, A. & Nagai, Y. (2001). Solitons in multi-level cellular automata. *Chaos Solit Fract*, in press.
- Beason-Held, L. L., Purpura, K. P., Krasuski, J. S., Desmond, R. E., Mangot, D. J., Daly, E. M., Optican, L. M., Rapoport, S. I., & VanMeter, J. W. (2000). Striate cortex in humans demonstrates the relationship between activation and variations in visual form. *Experimental Brain Research*, 130, 221–226.
- Beason-Held, L. L., Purpura, K. P., Krasuski, J. S., Maisog, J. M., Daly, E. M., Mangot, D. J., Desmond, R. E., Optican, L. M., Schapiro, M. B., & VanMeter, J. W. (1998). Cortical regions involved in visual texture perception: a fMRI study. *Brain Research. Cognitive Brain Research*, 7, 111–118.
- Beason-Held, L. L., Purpura, K. P., Van Meter, J. W., Azari, N. P., Mangot, D. J., Optican, L. M., Mentis, M. J., Alexander, G. E., Grady, C. L., Horwitz, B., Rapoport, S. I., & Schapiro, M. B. (1998). PET reveals occipitotemporal pathway activation during elementary form perception in humans. *Visual Neuroscience*, 15, 503–510.
- Beck, J. (1983). Textural segmentation, second-order statistics, and textural elements. *Biological Cybernetics*, 48, 125–130.
- Beck, J., Sutter, A., & Ivry, R. (1987). Spatial frequency channels and perceptual grouping in texture segregation. *Computer Visual Graph Image Process*, 37, 299–325.
- Blackman, R. & Tukey, J. Section B.5. Particular pairs of windows. The measurement of power spectra from the point of view of communications engineering, New York, Dover Publications: 95–100.
- Caelli, T., & Julesz, B. (1978). On perceptual analyzers underlying visual texture discrimination: part I. *Biological Cybernetics*, 28, 167–175.
- Caelli, T., & Julesz, B. (1979). Psychophysical evidence for global feature processing in visual texture discrimination. *Journal of Optical Society of America*, 69, 675–678.
- Caelli, T., Julesz, B., & Gilbert, E. (1978). On perceptual analyzers underlying visual texture discrimination: part II. *Biological Cybernetics*, 29, 201–214.
- Caelli, T., Rentschler, I., & Scheidler, W. (1987). Visual pattern recognition in humans. I. Evidence for adaptive filtering. *Biological Cybernetics*, 57, 233–240.
- Carandini, M., & Heeger, D. J. (1994). Summation and division by neurons in primate visual cortex. *Science*, 264, 1333–1336.
- Carandini, M., Heeger, D. J., & Movshon, J. A. (1997). Linearity and normalization in simple cells of the macaque primary visual cortex. *Journal of Neuroscience*, 17, 8621–8644.
- Chen, C. C., Kasamatsu, T., Polat, U., & Norcia, A. M. (2001). Contrast response characteristics of long-range lateral interactions in cat striate cortex. *Neuroreport*, 12, 655–661.
- Chubb, C., & Sperling, G. (1991). Texture quilts: basic tools for studying motion-from-texture. *Journal Mathematical Psychology*, 35, 411–442.
- Dreher, B., Michalski, A., Ho, R. H. T., Lee, C. W. F., & Burke, W. (1993). Processing of form and motion in area 21a of cat visual cortex. *Visual Neuroscience*, 10, 93–115.
- Emerson, R. C., Bergen, J. R., & Adelson, E. H. (1992). Directionally selective complex cells and the computation of motion energy in cat visual cortex. *Vision Research*, 32, 203–218.
- Gagalowicz, A. (1981). A new method for texture fields synthesis: some applications to the study of human vision. *IEEE Transactions Pat. Analysis Mach. International*, 3, 520–533.
- Geisler, W. S., & Chou, K. L. (1995). Separation of low-level and high-level factors in complex tasks: visual search. *Psychol. Rev.*, 102, 356–378.
- Geisler, W. S., & Hamilton, D. B. (1986). Sampling-theory analysis of spatial vision. *Journal of Optical Society of America A*, 3, 62–70.
- Gilbert, E. N. (1980). Random colorings of a lattice on squares in the plane. *SIAM Journal of Algebra Diseases Meth.*, 1, 152–159.

- Graham, N., & Sutter, A. (1996). Effect of spatial scale and background luminance on the intensive and spatial nonlinearities in texture segregation. *Vision Research*, *36*, 1371–1390.
- Graham, N., & Sutter, A. (1998). Spatial summation in simple (Fourier) and complex (non-Fourier) texture channels. *Vision Research*, *38*, 231–257.
- Graham, N., & Sutter, A. (2000). Normalization: contrast-gain control in simple (Fourier) and complex (non-Fourier) pathways of pattern vision. *Vision Research*, *40*, 2737–2762.
- Graham, N., Sutter, A., Venkatesan, C., & Humaran, M. (1992). Non-linear processes in perceived region segregation: orientation selectivity of complex channels. *Ophthalmic and Physiological Optics*, *12*, 142–146.
- Gurnsey, R., & Browse, R. A. (1987). Micropattern properties and presentation conditions influencing visual texture discrimination. *Perception and Psychophysics*, *41*, 239–252.
- Gurnsey, R., & Browse, R. A. (1989). Asymmetries in visual texture discrimination. *Spatial Vision*, *4*, 31–44.
- Howe, D. A., & Percival, D. B. (1995). Wavelet variance, Allan variance, and leakage. *IEEE Transactions Inst. Measurement*, *44*, 94–97.
- Johnson, R. A., & Wichern, D. W. (1992). *Applied multivariate statistical analysis*. New Jersey: Prentice Hall.
- Julesz, B. (1980). Spatial nonlinearities in the instantaneous perception of textures with identical power spectra. *Philosophical Transactions of Royal Society of London. Series B: Biological Sciences*, *290*, 83–94.
- Julesz, B. (1981). Textons, the elements of texture perception, and their interactions. *Nature*, *290*, 91–97.
- Julesz, B., Gilbert, E. N., Shep, L. A., & Frisch, H. L. (1973). Inability of humans to discriminate between visual textures that agree in second-order statistics—revisited. *Perception*, *2*, 391–405.
- Julesz, B., Gilbert, E. N., & Victor, J. D. (1978). Visual discrimination of textures with identical third-order statistics. *Biological Cybernetics*, *31*, 137–140.
- Jüttner, M., & Rentschler, I. (1996). Reduced perceptual dimensionality in extrafoveal vision. *Vision Research*, *36*, 1007–1022.
- Jüttner, M., & Rentschler, I. (2000). Scale-invariant superiority of foveal vision in perceptual categorization. *European Journal of Neuroscience*, *12*, 353–359.
- Kingdom, F. A., Keeble, D., & Moulden, B. (1995). Sensitivity to orientation modulation in micropattern-based textures. *Vision Research*, *35*, 79–91.
- Klein, S. A., & Tyler, C. W. (1986). Phase discrimination of compound gratings: generalized autocorrelation analysis. *Journal of Optical Society of America A*, *3*, 868–879.
- Landy, M. S., & Bergen, J. R. (1991). Texture segregation and orientation gradient. *Vision Research*, *31*, 679–691.
- Laws, K. I. (1980). Rapid texture identification. *SPIE*, *238*, 376–380.
- Lee, T.-W., Girolami, M., Bell, A. J., & Sejnowski, T. J. (2000). A unifying information-theoretic framework for independent component analysis. *Comput. Math. App.*, *31*, 1–21.
- Maddess, T., Davey, M., & Yang, E. (1999a). Discrimination of complex textures by bees. *J. Comp. Physiol. A*, *184*, 107–177.
- Maddess, T., Goldberg, I., Wine, S., Dobinson, J., Welsh, A. H., & James, A. C. (1999b). Testing for glaucoma with the spatial frequency doubling illusion. *Vision Research*, *39*, 4258–4273.
- Maddess, T., James, A. C., Goldberg, I., Wine, S., & Dobinson, J. (2000). A frequency doubling illusion based multiregion PERG for glaucoma. *Investigative Ophthalmology and Visual Science*, *41*, 3818–3826.
- Maddess, T., & Kulikowski, J. (1999). Apparent fineness of stationary compound gratings. *Vision Research*, *39*, 3404–3416.
- Maddess, T., McCourt, M. E., Blakeslee, B., & Cunningham, R. B. (1988). Factors governing the adaptation of cells in area-17 of the cat visual cortex. *Biological Cybernetics*, *59*, 229–236.
- Malik, J., & Perona, P. (1990). Preattentive texture discrimination with early vision mechanisms. *Journal of Optical Society of America A*, *7*, 923–932.
- Nagai, Y., Maddess, T., & Ankiewicz, A. (2001). Discrete algebra on cellular automata and binary textures. *Mem. Kokushikan U Cent. Inform. Sci.*, *22*, 51–64.
- Ohzawa, I., DeAngelis, G. C., & Freeman, R. D. (1997). Encoding of binocular disparity by complex cells in the cat's visual cortex. *Journal of Neurophysiology*, *77*, 2879–2909.
- Polat, U., Mizobe, K., Pettet, M. W., Kasamatsu, T., & Norcia, A. M. (1998). Collinear stimuli regulate visual responses depending on cell's contrast threshold. *Nature*, *391*, 580–584.
- Purpura, K. P., Victor, J. D., & Katz, E. (1994). Striate cortex extracts higher-order spatial correlations from visual textures. *Proceedings of the National Academy of Sciences of the United States of America*, *91*, 8482–8486.
- Räth, C., & Morfill, G. (1997). Texture detection and discrimination with anisotropic scaling indices. *Journal of Optical Society of America A*, *14*, 3208–3215.
- Rentschler, I., Jüttner, M., & Caelli, T. (1994). Probabilistic analysis of human supervised learning and classification. *Vision Research*, *34*, 669–687.
- Rubenstein, B. S., & Sagi, D. (1990). Spatial variability as a limiting factor in texture-discrimination tasks: implications for performance asymmetries. *Journal of Optical Society of America A*, *7*, 1632–1643.
- Schölkopf, B., Smola, A., & Müller, K.-R. (1998). Nonlinear component analysis as a kernel eigenvalue problem. *Neural Comp.*, *10*, 1299–1319.
- Sutter, A., Beck, J., & Graham, N. (1989). Contrast and spatial variables in texture segregation: testing a simple spatial-frequency channels model. *Perception and Psychophysics*, *46*, 312–332.
- Treisman, A., & Gormican, S. (1988). Feature analysis in early vision: evidence from search asymmetries. *Psychol. Rev.*, *95*, 15–48.
- Turano, K., & Pantle, A. (1989). On the mechanism that encodes the movement of contrast variations: velocity discrimination. *Vision Research*, *29*, 207–221.
- Victor, J. D. (1985). Complex visual textures as a tool for studying the VEP. *Vision Research*, *25*, 1811–1827.
- Victor, J. D. (1994). Images, statistics and textures: implications of triple correlation uniqueness for texture statistics and the Julesz conjecture: comment. *Journal of Optical Society of America*, *A11*, 1680–1684.
- Victor, J. D., & Conte, M. M. (1989). Cortical interactions in texture processing: scale and dynamics. *Visual Neurosciences*, *2*, 297–313.
- Victor, J. D., & Conte, M. M. (1990). Motion mechanisms have only limited access to form information. *Vision Research*, *30*, 289–301.
- Victor, J. D., & Conte, M. M. (1991). Spatial organization of nonlinear interactions in form perception. *Vision Research*, *31*, 1457–1488.
- Victor, J. D., & Zemon, V. (1985). The human visual evoked potential: analysis of components due to elementary and complex aspects of form. *Vision Research*, *25*, 1829–1842.
- Watson, A. B. (1987). Efficiency of a model human image code. *Journal of Optical Society of America A*, *4*, 2401–2417.
- Werkhoven, P., Sperling, G., & Chubb, C. (1993). The dimensionality of texture-defined motion: a single channel theory. *Vision Research*, *33*, 463–485.
- Werkhoven, P., Sperling, G., & Chubb, C. (1994). Perception of apparent motion between dissimilar gratings: spatiotemporal properties. *Vision Research*, *34*, 2741–2759.

- Yamaguchi, H., & Nagai, Y. (1998). Correlation dimension as the large deviation for distribution of distances between two points on an embedded manifold. *J. Phys. Soc. Japan*, *10*, 3397–3404.
- Yang, E. C., & Maddess, T. (1997). Orientation-sensitive neurons in the brain of the honeybee (*Apis mellifera*). *Journal of Insect Physiology*, *43*, 329–336.
- Yellott, J. I. (1993). Implications of triple correlation uniqueness for texture statistics and the Julesz conjecture. *Journal of Optical Society of America A*, *10*, 777–793.
- Zanker, J. M. (1996). On the elementary mechanism underlying secondary motion processing. *Philosophical Transactions of Royal Society of London. Series B*, *351*, 1725–1736.